Bachelor Thesis

Hydrodynamic Analysis of the Installation of a Gravity Based Foundation of Offshore Wind Turbine Generators

Hydrodynamische Analyse der Installation einer Schwergewichtsgründung für Offshore-Windkraftanlagen

Autor: Marvin Phillip Bense
Matrikelnummer: 313460

Aufgabensteller: Prof. Dr.-Ing. Andrés Cura Hochbaum
Fachgebiet Dynamik Maritimer Systeme
Institute für Land und Seeverkehrt
Technische Universität Berlin

Betreuer: Dr.-Ing. Florian Stempinski
HOCHTIEF Solutions AG
Civil Engineering and Marine Works

Thema zum Vertiefungsmodul: Schiffshydrodynamik I

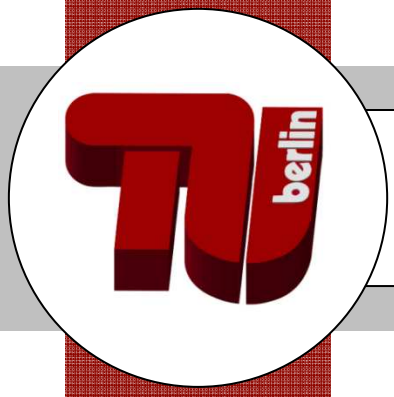

Technische Universität Berlin – Institut für Land- und Seeverkehr

Salzufer 17-19, 10587 Berlin

www.marsys.tu-berlin.de

Eingereicht am: 5. Dezember 2011

Eidesstattliche Erklärung

(Declaration of Academic Honesty)

Die selbständige und eigenhändige Ausfertigung versichert an Eides statt

Berlin, den 05. Dezember 2011

_____

Marvin Phillip Bense, 313460

Task Description

HOCHTIEF Solutions AG in cooperation with Arup and Costain is developing a gravity based foundation as an alternative concept to conventional foundation types of WTGs (wind turbine generators). The foundation consists of a self-floating concrete structure that is towed to its location and lowered to the sea bed by a controlled ballasting process. A targeted installation area is the North Sea up to 150 nautical miles off the coast of the UK with water depths between 30 and 40 m.

The objective of this thesis is to determine the static and dynamic behaviour of the foundation during construction, towing to the location, and installation offshore. The compliance with concurrent offshore codes has to be checked and possible design improvements are to be suggested.

The following steps have to be completed:

1. Write a short introduction covering the state of the art of foundations for WTGs including their installation
2. Describe the current state of the design of the self floating concrete structure including the installation and decommissioning concept.
3. Describe the methods used by AQWA to calculate forces and motions.
4. Conduct spatial and temporal convergence tests in order to prove consistency in the generated model and simulations.
5. Conduct an analysis of the hydrostatics during all transport and installation stages. Are all safety requirements met?
6. Determine a hydrodynamic analysis to determine motions (ROAs and significant motions) and drift forces in seaway (frequency domain) during towing and installation. Suggest limiting sea states for the transport and installation operations.
7. Based on the critical states determined above carry out motion analyses in time domain to quantify the nonlinear motion behaviour in critical sea states (towage, holding condition, installation stages).

To carry out the calculations the software packages ANSYS AQWA and Autohydro as well as all design data of the structure are provided. Intermediate results are to be discussed with the supervisor at regular intervals. After completion the final results are to be presented to members of the staff in a presentation of approx. 20 min.

Abstract

The Scope of this thesis is the motion analysis of a gravity based foundation (GBF) for offshore wind turbine generators (WTGs). Since the foundation is self buoyant, only standard tug boats are required for offshore towage and installation. The GBF is lowered to the seabed by a controlled influx of water into 9 inner ballast tanks. All analyses are conducted for transit and a range of drafts during the installation.

The hydrostatic analysis proves that the GBF is definite in form for drafts up to 15 m and definite in weight for greater drafts. Based on hydrostatic data and with consideration of viscous damping the response amplification factors (RAOs) are calculated in the frequency domain by AQWA. The Results are in accordance with model tests and hand calculations. In addition mean drift forces are determined. The RAOs are used to determine significant and maximum motions for a range of wave spectra. In a towing analysis the minimum towing pull required (TPR) and the maximum inclination are determined. The hydrodynamic analysis of the GBF shows suitable motion behaviour for towage and installation in 2 m significant wave height.

Kurzfassung

Aufgabenstellung dieser Arbeit ist die Bewegungsanalyse einer Schwerkraftgründung (GBF) für Offshore Windkraftanlagen (WTGs). Durch die Schwimmfähigkeit des Fundaments werden für den Transport sowie die Installation ausschließlich Standardschleppern benötigt. Das Absenken wird durch einen kontrollierten Zufluss von Wasser in die 9 inneren Ballasttanks erzielt.

Die hydrostatische Analyse zeigt, dass das GBF bei Tiefgängen bis 15 m formstabil ist und bei größeren Tiefgängen gewichtsstabil wird. Basierend auf den hydrostatischen Daten und unter Berücksichtigung der viskosen Dämpfung werden die Übertragungsfunktionen (RAOs) im Frequenzbereich bestimmt. Die Ergebnisse stimmen mit Modellversuchen und Handberechnungen überein. Die RAOs werden zur Bestimmung von signifikanten und maximalen Bewegungen für eine Reihe von Wellenspektren berechnet. In einer Schleppanalyse werden die minimal benötigte Schleppkraft (TPR) und die maximale Neigung bestimmt. Die hydrodynamische Analyse zeigt gute Bewegungseigenschaften der GBF während des Schleppens und der Installation in 2 m signifikantem Seegang.

Table of Content

1 Introduction

Offshore wind energy is a rapidly growing market with an increasing demand for inexpensive wind turbine generator (WTG) foundations. Their installation must be as simple and cost effective as possible. For the upcoming projects they are needed in large quantities and have to accommodate the increasing WTG size. In addition, the strict requirements on safety and environmentally pollution have to be met.

With the concrete gravity based foundation (GBF), developed by Arup, Constain and HOCHTIEF, these needs and requirements are targeted. The significant benefits of this foundation are installation and decommission methods, independent from heave lifting offshore cranes as well as the realisation of mass production. If a reduced weather dependency of the installation operations can be proven, the installation season is extended. The GBF design is aiming at the UK Round 3 wind farm projects. Large scale application, including other countries, is intended by realization of mass production. In the German territorial waters GBFs are currently not permitted by law, due to the sealing of the seabed and the inferior collision characteristics. For this reason application in German wind farm projects is not planned at this time.

In order to determine motion characteristics of a floating structure it is common to perform numerical simulations. With this approach reliable results can be produced. The benefit of numerical simulations is their cost efficiency and fast results. This way the potential of optimisations can be determined early in the design process.

1.1 Types of Foundation for Offshore Wind Turbines

A WTG foundation has to transmit forces and moments to the structure into the seabed. They have to withstand the extreme offshore conditions induced by wind, waves, current and ice. Other aspects such as corrosion, scour, collision with marine vessels and decommissioning must be taken into account when designing a foundation with an operational life of approximately 25 years (Arup, Constain, HOCHTIEF, 2011).

Foundation types for offshore wind turbines are: jacket, tripod, tripile, monopile, concrete gravity base, suction caisson[1] and hybrid gravity based foundations as shown in Figure 1. Scour protection, in the form of gravel layers around the foundation may be required for all foundation types depending on ground conditions.

[1] or suction bucket

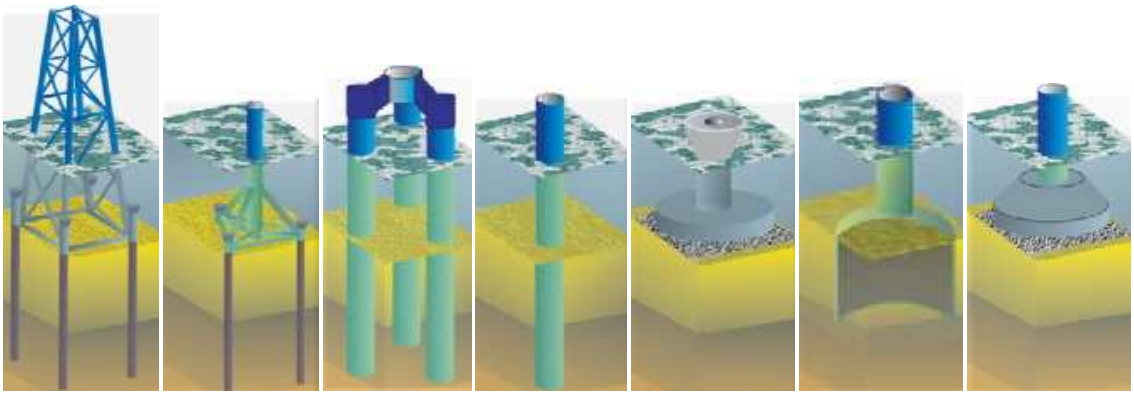

Figure 1: Types of foundations – jacket, tripod, tripile, monopile, concrete gravity base, suction caisson, hybrid gravity base (from left to right) (HOCHTIEF Solutions AG, 2011)

1.1.1 Common Types of Foundations

So far jackets, tripods, tripiles, monopiles and gravity based foundations have been successfully installed in wind farm projects. These foundation types, except the GBF, require deeper soil penetration to ensure sufficient structural stability. This is generally achieved by piling or drilling long piles into the seabed. Piles are guided by the pile sleeves located at the contact patches of the foundation. After piling is completed they are fixed to the structure by grouting. When monopiles are used most of structure has to be embedded into the ground. The duration of the piling process depends significantly on pile diameter and pile depth. The downside of the piling procedure is the intensive noise generation with a severe impact on the marine life. For that reason strict limitations are imposed both on noise intensity and execution time over the year. Noise reduction can be achieved by applying bubble curtains but their application is complex. (Deutsche Energie-Agentur GmbH (dena), 2009)

Figure 2: Jackets for large water depths, tripod used in cooperation with Weserwind and monopile for low water depths (from left to right) (HOCHTIEF Solutions AG, 2011)

As seen in Table 1 monopiles are suitable for relatively low water depths and their dimensions depend significantly on the soil condition. Problems with grouting and scour protection have to be considered as well. Their advantage lies in their sim-

plicity and robustness. Monopiles are collision friendly since they are able to bend in case of an incident, thus reducing the damage to the ship. For offshore transport purposes they can be made buoyant by sealing the ends with special lids allowing a wet towage to the installation site.

WTG Size	3.6 MW	6.0 MW
Water Depth	≤ 30 m	≤ 22 m
Diameter up to	∅ 6.50 m	∅ 6.50 m
Wall Thickness	70 – 120 mm	70 – 120 mm
Length up to	70 m	60 m
Weight up to	800 t	800 t

Table 1: Typical dimensions of monopiles in current windparks

At water depths or soil conditions where monopiles are not applicable (Table 1) jackets, tripods or triples are used. They are relatively light structures and require small piles in relation to the length of the monopile. Due to their complex geometry their construction costs are high. Since jackets, tripods and tripiles have three or four contact patches the levelling of these foundation types is more complex as well. Furthermore they have to be transported by means of marine vessels to their installation site. This represents a logistical challenge due to their outer dimensions.

These foundation types and monopiles require cranes to be adequately positioned and installed. Offshore cranes and other purpose-built installation vessels and equipment are limited and expensive. Additionally, their installation processes depend highly on weather conditions resulting in large numbers of WOW (waiting on weather) days per year. This circumstance requires very intensive and accurate preparatory work and has led to significant delay in recent wind farm installation. A tripod installation with the BHO-Innovation for example is assumed to have a total of 89 WOW days over the year with an accumulation of WOW days between October and March (Dasdeler, 2011).

1.1.2 GBF

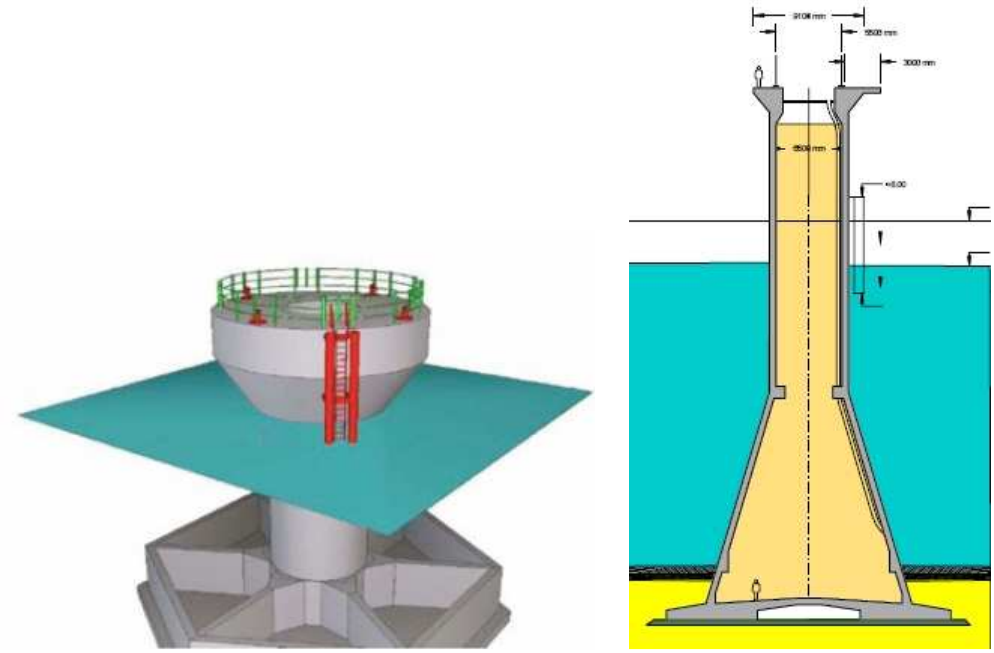

Figure 3: Gravity based foundations from Lillgrund and Thornton Bank (from left to right) (Arup, Constain, HOCHTIEF, 2011)

In contrast to other foundation types forces and moments on a GBF are transmitted mainly over the horizontal contact area between seabed and foundation base. The mass of the structure and the vertical force resulting from the water pressure on its surface have to be large enough to prevent the structure from tipping. Horizontal forces are also transmitted to the foundation base.

The penetration depth of the skirts is relatively low therefore the condition of the deeper soil layers, like load capacity and the presence of erratic blocks, can be disregarded. GBFs are made predominantly of reinforced concrete and normally need ballast to obtain the required mass. Ballasting is achieved by filling inner or outer compartments with water and/or solid ballast, in form of sand or rocks.

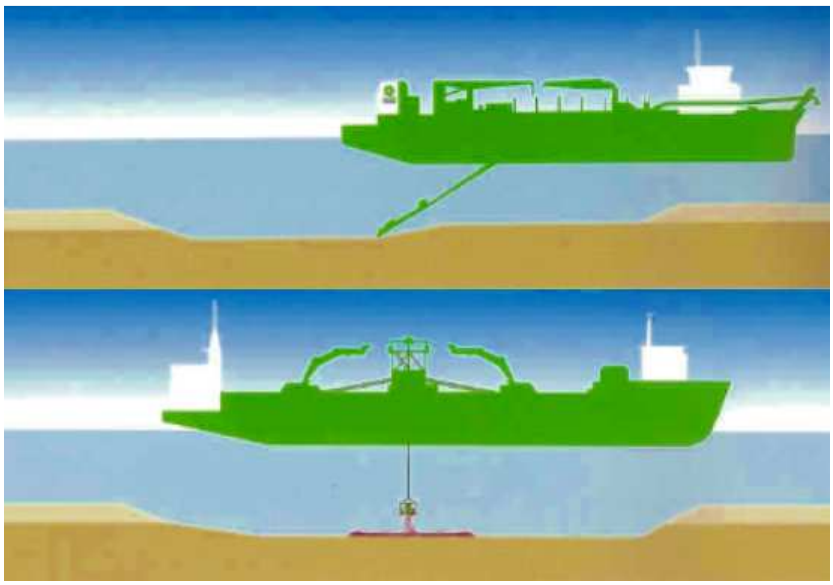

Figure 4: Dredger and fall-pipe vessels (from top to bottom)

In order to achieve the required ground properties for a safe stand of the GBF intensive preparatory work has to be conducted. This includes removal and levelling of the top soil and application of special ground material to reach adequate load capacity involving dredgers and fall-pipe vessels. After the GBF is set down the excavation is refilled and the scour protection is applied. The material costs of the concrete GBF are relatively low and protective measures in form of an increased wall thickness is not required.

1.2 GBF Design

The gravity based foundation prototype developed by Arup, Constain and HOCHTIEF is made of reinforced concrete and is designed for a water depth of 35 m representing the average water depth in the Hornsea area. With adaptations the GBF is intended to be installed in water depths between 20 m and 55 m. The structure is hollow and self buoyant without the requirement of additional buoyancy aids. This key characteristic allows an offshore towage from the port of production to the wind farm by means of standard tug boats. Mooring points for towage and installation are located on top of the base slab (Figure 6).

Length [m]	31.00
Breadth [m]	31.00
Height [m]	55.70
Transit Draft [m]	8.81
Light Weight [t]	6961.6
Installation Water Depth [m]	35.00

Table 2: GBF main dimensions

The installation procedure is initiated by a controlled influx of water into the foundation, slowly lowering it to the seabed in an intended 6 to 8 hour time frame. A controlled rate of submergence is crucial particularly during the period when only the narrow column is above sea level. For installation purposes the GBF has 9 tanks located in the socket which are open at the top (Figure 5 and Figure 6). Their function is to insure sufficient stability by reducing the free surface moments of the ballast water in the structure.

In addition, they can be used for corrections of the floating position. Initially only the central tank is filled to a water level of 8.7 m. Then the 8 outer tanks are evenly flooded until all tanks are equally filled to a water level of 8.7 m. From there on water levels in the tanks increase equally until the structure has reached the required ballast mass. During this installation the foundation is kept in place by the tug boats until it is safely positioned on the seabed. The obtained ballast weight is sufficient to ensure a safe stand of the foundation without WTG in storm conditions. For further increase of weight, sand ballast is added or substituted for the water ballast.

The installation is realised without any instrumentation and automatic control. Neither divers, ROVs nor man access within the base during installation are required. Sea-borne noise and vibration are minimised as well, so installation can proceed year-round. This transport and installation procedure requiring only tug boats

represents a significant increase in efficiency and savings by reducing complexity, risk of component failure and installation time. If this process proves to be less weather dependent, which is the goal of the thesis, the installation season is extended (Figure 8).

Since the internal volume is isolated from the sea on completion, the GBF can easily be decommissioned by reversing the installation procedure. This allows a sustainable renaturation of the installation site. Repowering[2] is also possible with the developed GBF. The analysed foundation has the dimensions described in Table 2 and Figure 5 and can be divided into the following substructures:

- skirt
- base slab
- socket containing 9 ballast chambers
- (large) lower cone
- (small) upper cone
- shaft with ladder and transition piece

[2] Exchange of the WTG without the need for foundation

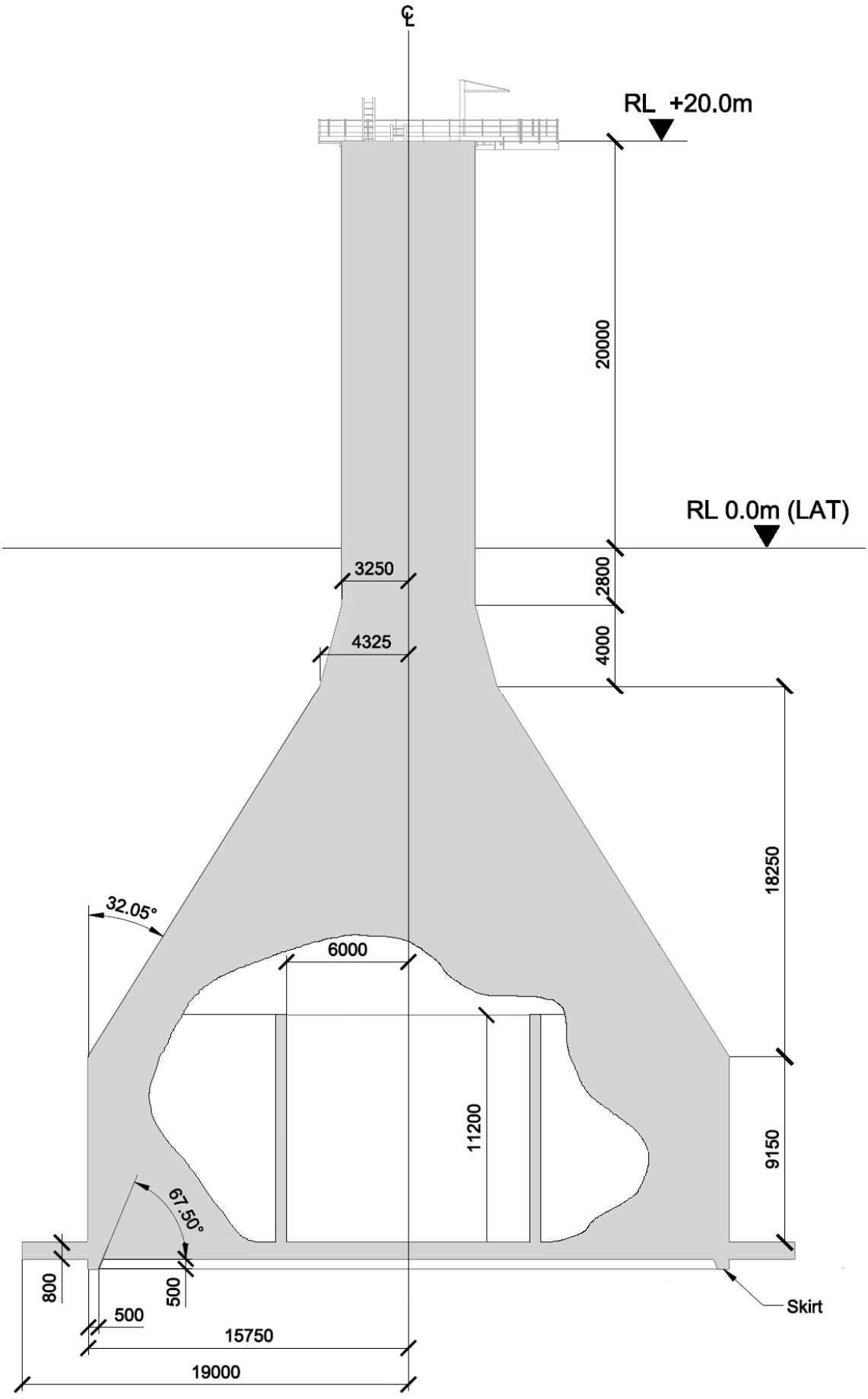
℄
RL +20.0m
20000
RL 0.0m (LAT)
3250
2800
4325
4000
18250
32.05°
6000
11200
9150
67.50°
800
500
500
Skirt
15750
19000

Figure 5: GBF outline

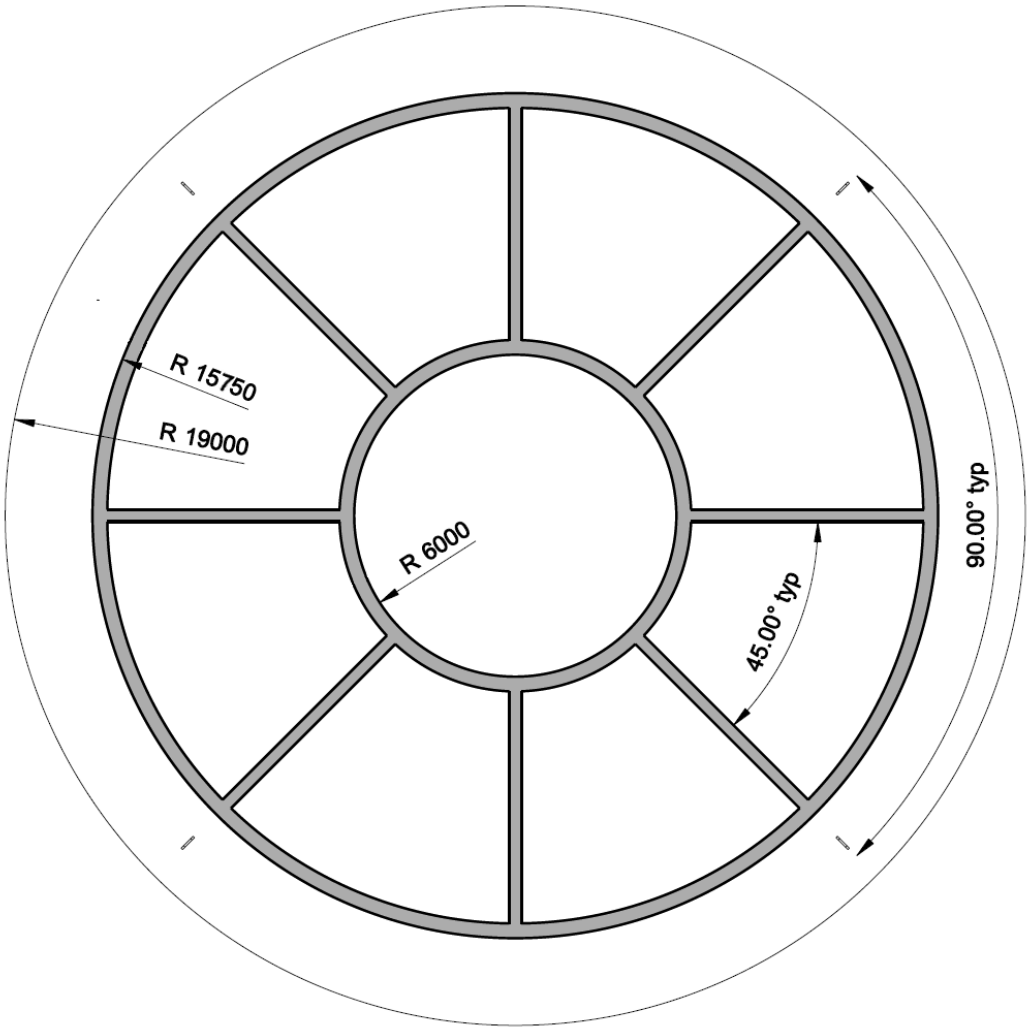

Figure 6: Tank plan

1.3 Design Bases

The design bases are described in the Design Bases Rev B report (Arup, Constain, HOCHTIEF, 2011).

1.3.1 Location Characteristics

The wind farm is assumed to be located in Zone 3, 4 or 5 of the UK Round 3 licence area. The Hornsea area (Zone 4) with a 4GW of development potential is considered to be appropriate for design development.

Total zone area	4,735 km²
Distance to Yorkshire coast	31 - 190 km
Water depth in the zone	Average: 30 - 40 m max.: 70 m

Table 3: Hornsea key facts (SMart Wind, 2011)

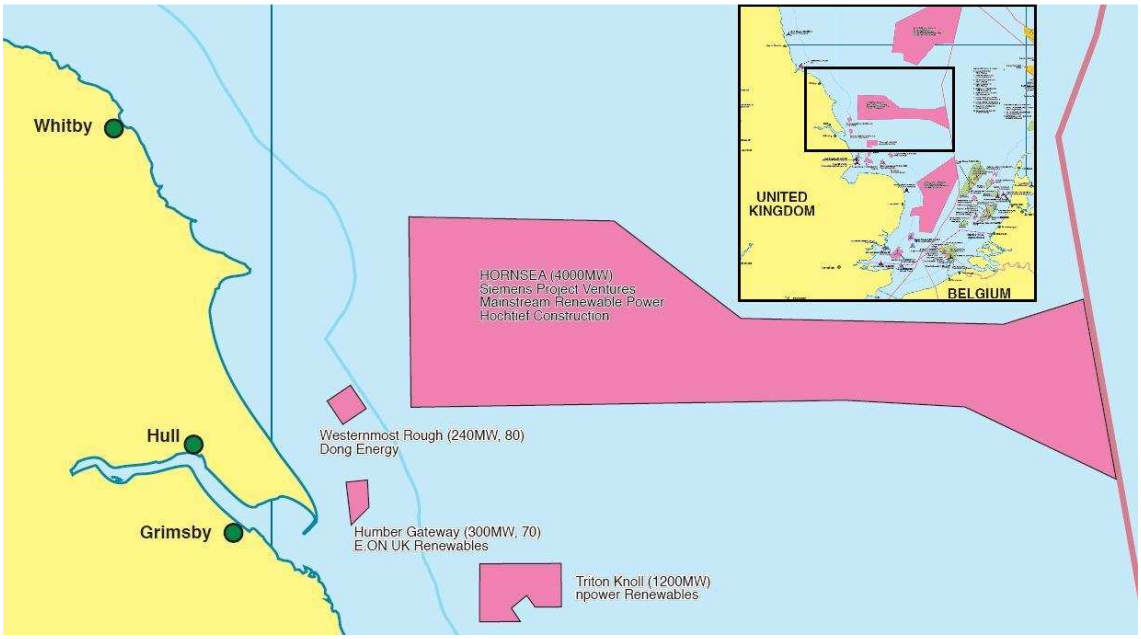

Figure 7: Map of Hornsea (European Wind Energy Association (EWEA), 2009)

1.3.2 Environmental Conditions

Environmental conditions are taken in the Western part of the Hornsea area (MetOcean). These are 100 year values which are considered to provide conservative conditions for the majority of Round 3 areas. The data shown in Table 4 is interpolated using data from EN ISO 19901-1:2005.

Return period (years)	1	50	100
10 min mean wind speed [m/s]	28.2	31.6	35.3
Significant wave height H_S [m]	7.2	8.4	10.0
Maximum wave height[3] H_{max} [m]	13.4	15.6	18.6
Spectral peak period T_p [s]	12.0	13.0	14.3

Table 4: Wind and wave data for the 1-, 50- and 100-year-return-period storm

The one minute mean wind speed at 10 m above LAT (lowest astronomical height) [4] is 37 m/s. The non-exceedance of 1 m, 2 m and 4 m significant wave height over one year is shown in Figure 8. It is intended to install and tow the GBF in 2 m significant wave height.

[3] For a wave train of 1000 waves

[4] This value is given in the Design Bases Rev B report. Note that it is considered as very conservative value for towing calculations. It exceeds the 1 year-return-period storm with a wind speed of 28.2 m/s and the holding condition with a wind speed of 20 m/s.

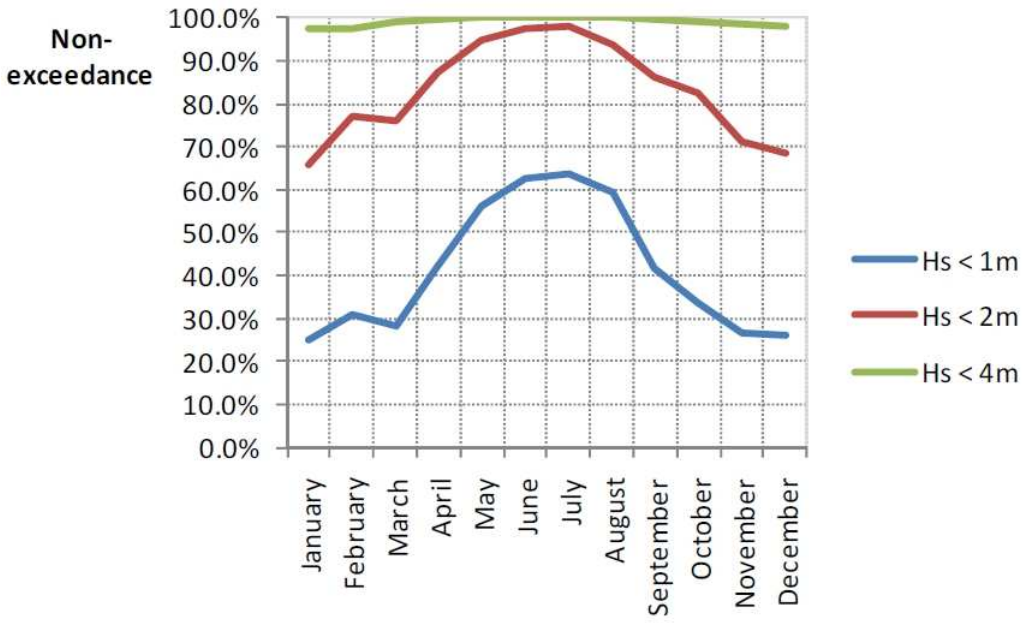

Figure 8: Non-exceedance of H_S over year (Arup, Constain, HOCHTIEF, 2011)

The general geotechnical conditions across the Hornsea area are sand or gravel deposits overlying glacial deposits. In the eastern area there are some infilled glacial valleys which would be unsuitable for gravity foundations without ground preparation. In the western areas, mobile sand waves are present which may also make placing gravity foundations more complex.

2 Theory

In this section the applied hydrostatic and hydrodynamic methods are described. In addition, the characteristics of the simulation software AQWA are explained (Birk, 2001).

2.1 Hydrostatic Analysis

A free floating structure at equilibrium displaces an amount of water equal to the weight of the structure. The displacement of water creates a pressure field on the surface of the structure. The resulting buoyant force is directed vertically in direction of the positive z axis[5] and is determined by

$$F_B = F_G = \rho \cdot g \cdot \mathrm{V} \tag{2.1}$$

and acts through the centre of buoyancy (COB). COB is determined the centre-of-volume theorem with reference to keel K:

$$x_{B_0} = \frac{\sum_{i=1}^{n} V_i \cdot x_{Bi}}{V}, \qquad y_{B_0} = \frac{\sum_{i=1}^{n} V_i \cdot y_{Bi}}{V}$$
$$z_{B_0} = \overline{KB}_0 = \frac{\sum_{i=1}^{n} V_i \cdot z_{Bi}}{V} \tag{2.2}$$

The weight force counteracts through the centre of gravity G. At equilibrium both forces act inversely to each other on the same vertical line through G and B_0.

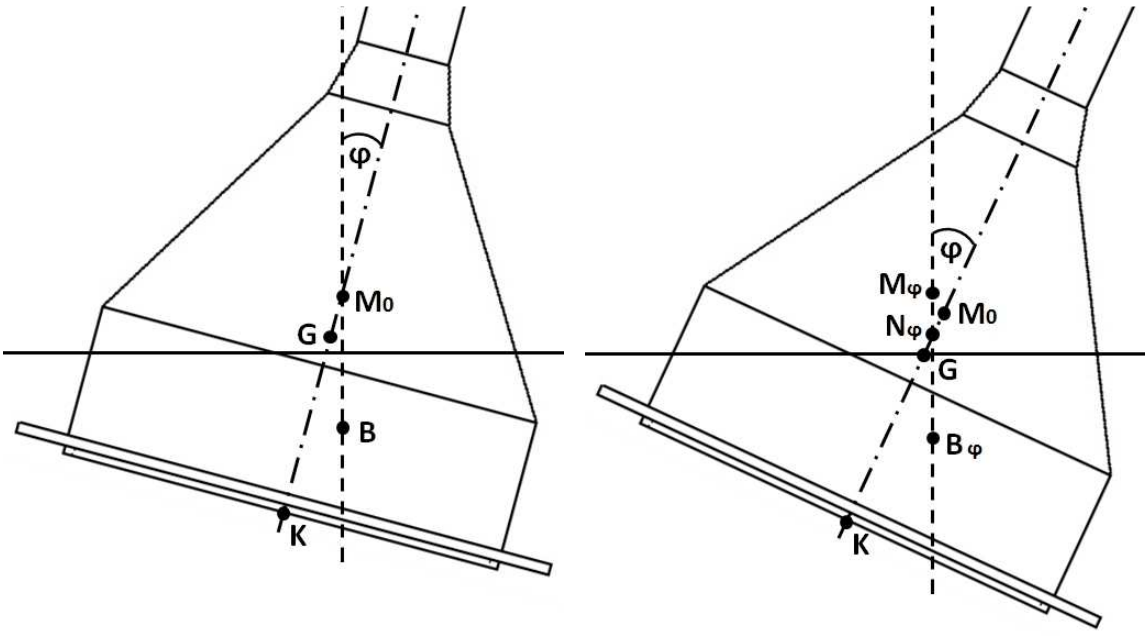

Figure 9: Initial stability (left) and large angle stability (right)

If the structure is heeled (φ), the geometry of the displaced fluid volume changes, the centre of buoyancy is shifted from its initial location B_0 to B_φ and a new waterline is defined. The new action line of the buoyancy force is shifted, with respect to

[5] z is defined in opposite direction as gravity with its origin in the still water surface

the line of action of the weight force, by the righting lever $\overline{GZ}_\varphi$ of static stability. At small inclination angles ($\varphi \ll 1°$) righting moment is determined by

$$M_R = F_B \cdot \overline{GM}_0 \cdot sin\,\varphi \tag{2.3}$$

with the initial metacentre M_0 defined as the intersection of action lines of the trimmed buoyancy force B_φ with the initial buoyancy force B_0. The initial metacentric height $\overline{\mathrm{GM}}_0$ of a floating structure is defined by

$$\overline{GM}_0 = \overline{BM}_0 + \overline{KB}_0 - \overline{KG} \tag{2.4}$$

with

$$\overline{BM}_0 = \frac{I_T - \sum \frac{\rho_{Ballast}}{\rho} \cdot I_{Ti}}{V} \tag{2.5}$$

The moments of the water plane area in transversal and longitudinal direction, I_T and I_L, are defined as:

$$I_T = \iint_{A_{WL}} y^2\,dA \qquad\qquad I_L = \iint_{A_{WL}} x^2\,dA \tag{2.6}$$

With further inclination the metacentre M_φ shifts depending on the shape of the structure. The metacentre M_φ is defined as the point at which adjacent vertical line through the heeled centre of buoyancy are crossing. The righting moment is defined as

$$\begin{aligned} M_R &= F_B \cdot \overline{GZ}_\varphi \\ &= \rho \cdot g \cdot V \cdot \left[\overline{GM}_0 + \overline{M_0 N}_\varphi\right] \cdot sin\,\varphi \end{aligned} \tag{2.7}$$

with N_φ defined as the point at which a vertical line through the heeled centre of buoyancy B_φ crosses the line through the original vertical centre of buoyancy B_0.

2.1.1 Definite in Form and Definite in Weight

Initial stability of a floating structure is divided into two cases:

- definite in form and
- definite in weight.

Definite in form applies when the magnitude of $\overline{BM}_0$ is sufficient, allowing the COG to be above the COB $\left(\overline{GB}_0 < 0\right)$ while initial stability $\overline{GM}_0$ is positive (See equation (2.4)). The equation represented in (2.5) shows that the relation of the moment of the water plane area $\mathrm{I_T}$ (or $\mathrm{I_L}$) to the displaced volume is decisive here. Additionally, the reduction of $\overline{BM}_0$ by the free surface effects has to be considered. To the contrary, definite in weight is given, when the COG is below the COB $\left(\overline{GB}_0 > 0\right)$.

In this case initial stability $\overline{GM_0}$ is positive even if $\overline{BM_0}$ is zero. Free surface effects must be considered and require a larger $\overline{BM_0}$ or a smaller $\overline{GB_0}$ respectively (Schneekluth, 1988).

2.1.2 Wind Heeling Moment

The wind heeling moment is defined by (IMO, 2009)

$$\begin{aligned} M_W &= h_{WP} \cdot F_W \cdot \cos^2 \varphi \\ &= h_{WP} \cdot c_h \cdot c_s \cdot \frac{\rho}{2} \cdot A_W \cdot v_W^2 \cdot \cos^2 \varphi \end{aligned} \tag{2.8}$$

The vertical lever of the wind overturning moment h_{WP} is messured from the centre of pressure of all surfaces exposed to the wind A_W to the centre of lateral resistance of the underwater body. The drag coefficient c_s depends on the shape of the respective body were as c_h accounts for a profiled wind speed. For most cases the body is composed of differently shaped substructures. In this case the sum of the overturning moments of each substructure is required. The overturning lever of wind is then

$$h_w = \frac{M_W}{F_B} \tag{2.9}$$

2.2 Hydrodynamic Analysis

The methods described in this section to determine the hydrodynamic characteristics of an arbitrary body are based on a linear approach of potential theory including the following assumptions

- The described fluid is ideal: It has no friction, is free of rotation and is incompressible
- The relative wave height is small $(k\zeta_a \sim H/L \ll 1)$

2.2.1 Linear Wave theory

The velocity potential of a singular regular wave in finite water depth is defined by the linear wave theory as

$$\Phi_0 = \frac{-i\zeta_a g}{\omega} \cdot \frac{cosh\big(k(z+d)\big)}{cosh(kd)} \cdot e^{i(k\chi - \omega t)} \tag{2.10}$$

with $\chi = x \cos\psi + y \sin\psi$. In linear wave theory convection is not considered thus fluid particles move on a closed cycle during a wave period. For deep water the potential is simplified to

$$\Phi_0 = \frac{-i\zeta_a g}{\omega} \cdot e^{kz} \cdot e^{i(k\chi - \omega t)} \tag{2.11}$$

The wave frequency ω is written as

$$\omega = \sqrt{kg\ tanh(kd)} \tag{2.12}$$

and the wave number k is

$$k = \frac{2\pi}{L} \tag{2.13}$$

2.2.2 Second Order Wave Theory

The velocity potential of a singular regular wave in finite water depth is defined by the stokes 2nd order wave theory as (Chen, 2006)

$$\begin{aligned}\Phi_0 = &\frac{-ig\zeta_a}{\omega} \cdot \frac{cosh\big(k(z+d)\big)}{\cosh(kd)} \cdot e^{i(k\chi - \omega t)} \\ &+ \frac{-i3\zeta_a^2\omega}{8} \cdot \frac{cosh\big(2k(z+d)\big)}{\sinh^4(k \cdot d)} \cdot e^{i2(k\chi - \omega t)} \\ &- \frac{gk\zeta_a^2}{4} \cdot \left[\frac{4S + 1 - \tanh^2(kd)}{4S^2 kd - \tanh(kd)}\right] t\end{aligned} \tag{2.14}$$

with

$$S = \frac{\sinh(2kd)}{2kd - \sinh(2kd)} \tag{2.15}$$

The 2nd order wave theory is more exact since convection is considered. Particles no longer move on closed cycles but on an open ellipse in the direction of wave propagation.

2.2.3 JONSWAP Spectrum

The JONSWAP[6] spectrum is applied as the standard wave spectrum for irregular sea states in the North Sea (Clauss G. , 1995). Examination of the spectrum shows that most of the wave energy is often concentrated in a relatively narrow band, which determines the actual wave pattern.

Parameterization of the classic form of the JONSWAP spectrum was undertaken by (Houmb & Overvik, 1976). This form is accepted by the AQWA suite. The peak frequency and the peak enhancement factor γ together with the empirical parameters termed α and R are used in this formulation. The spectral ordinate is $S(\omega)$ given by (ANSYS, Inc., 2009a):

$$S(\omega) = \frac{\alpha \cdot g^2 \cdot \gamma^R}{\omega^5} e^{-\frac{5}{4}\left[\frac{\omega_P}{\omega}\right]^4} \tag{2.16}$$

[6] Joint North Sea Wave Project

With
$$\alpha = 0.3395\left(\frac{H_s\omega_P^2}{g}\right)^{2.036}[1 - 0.298\ln\gamma] \tag{2.17}$$

$$R = e^{\frac{-(\omega-\omega_P)^2}{2\sigma^2\omega_P^2}} \tag{2.18}$$

$$\sigma = \begin{cases} 0.07 \text{ for } \omega \leq \omega_P \\ 0.09 \text{ for } \omega \geq \omega_P \end{cases} \tag{2.19}$$

With $\gamma = 3.3$ for the JONSWAP spectra the above equation simplifies to:

$$S(\omega) = 0.201 \cdot H_s^{2.036} \cdot \frac{\omega_P^{4.072}}{\omega^5} \cdot e^{-\frac{5}{4}\left[\frac{\omega_P}{\omega}\right]^4} \cdot 3.3^{\exp\left(-\frac{(\omega-\omega_P)^2}{2\sigma^2\omega_P^2}\right)} \tag{2.20}$$

2.2.4 Linear Differential Equation of Motion

The motion of a free floating rigid structure can be described by a differential equation based on the Newton's law of motion (Lewis, 1989). In matrix form for the 6 degrees of freedom it is written as

$$(\mathrm{M_s} + \mathrm{M_h}) \cdot \underline{\ddot{s}} + \mathrm{B} \cdot \underline{\dot{s}} + \mathrm{C} \cdot \underline{s} = \underline{\mathrm{F_e}} \tag{2.21}$$

with $\underline{s}$ as the vector of the of the rigid body position with its origin in the initial or equilibrium position of COG and $\underline{F_e}$ as the excitation force on the structure with its components $\underline{F_e}^T = (F_{ex}, F_{ey}, F_{ez}, M_{exx}, M_{eyy}, M_{ezz})$. The structural mass matrix $\mathrm{M_s}$ of a floating body with respect to COG is written as (Newmann, 1977):

$$\mathrm{M_s} = \begin{bmatrix} \mathrm{m} & 0 & 0 & 0 & 0 & 0 \\ 0 & \mathrm{m} & 0 & 0 & 0 & 0 \\ 0 & 0 & \mathrm{m} & 0 & 0 & 0 \\ 0 & 0 & 0 & \mathrm{I_{xx}} & 0 & 0 \\ 0 & 0 & 0 & 0 & \mathrm{I_{yy}} & 0 \\ 0 & 0 & 0 & 0 & 0 & \mathrm{I_{zz}} \end{bmatrix} \tag{2.22}$$

For a rotationally symmetric body in regard to the z axis the matrix of the hydrodynamic mass $\mathrm{M_h}$ is written as:

$$\mathrm{M_h} = \begin{bmatrix} \mathrm{m_{h11}} & 0 & 0 & 0 & \mathrm{m_{h15}} & 0 \\ 0 & \mathrm{m_{h22}} & 0 & \mathrm{m_{h24}} & 0 & 0 \\ 0 & 0 & \mathrm{m_{h33}} & 0 & 0 & 0 \\ 0 & \mathrm{m_{h42}} & 0 & \mathrm{m_{h44}} & 0 & 0 \\ \mathrm{m_{h51}} & 0 & 0 & 0 & \mathrm{m_{h55}} & 0 \\ 0 & 0 & 0 & 0 & 0 & \mathrm{m_{h66}} \end{bmatrix} \tag{2.23}$$

For the potential damping matrix B analogous assumptions can be made:

$$B = \begin{bmatrix} b_{11} & 0 & 0 & 0 & b_{15} & 0 \\ 0 & b_{22} & 0 & b_{24} & 0 & 0 \\ 0 & 0 & b_{33} & 0 & 0 & 0 \\ 0 & b_{42} & 0 & b_{44} & 0 & 0 \\ b_{51} & 0 & 0 & 0 & b_{55} & 0 \\ 0 & 0 & 0 & 0 & 0 & b_{66} \end{bmatrix} \tag{2.24}$$

The stiffness Matrix C of the structure at equilibrium is determined by cut water-plane area A_{WL} and the position of the COB ($\underline{x_B}$) and the COG ($\underline{x_G}$). The matrix is written for a rotationally symmetric body, in relation to z axis, with its COG located in axis rotation ($\underline{x_G} = (0, 0, z_G)$). In this case the centre of the water plane area is also located in the z axis ($x_{SWL} = y_{SWL} = 0$). The matrix is written as:

$$C = \rho \cdot g \cdot \begin{bmatrix} 0 & 0 & 0 & 0 & 0 & 0 \\ 0 & 0 & 0 & 0 & 0 & 0 \\ 0 & 0 & c_{33} & 0 & 0 & 0 \\ 0 & 0 & 0 & c_{44} & 0 & 0 \\ 0 & 0 & 0 & 0 & c_{55} & 0 \\ 0 & 0 & 0 & 0 & 0 & 0 \end{bmatrix} \tag{2.25}$$

with $c_{33} = A_{WL}$ $\qquad c_{34} = c_{43} = \int_A y_{SWL}\, dA = 0$

$$c_{35} = c_{53} = -\int_A x_{SWL}\, dA = 0 \qquad c_{44} = \int_A y^2\, dA + V(z_B - z_G) \tag{2.26}$$

$$c_{45} = c_{54} = -\int_A xy\, dA = 0 \qquad c_{55} = \int_A x^2\, dA + V(z_B - z_G)$$

The entries c_{44} and c_{55} are equal due to the symmetry. The vertical coordinate of the centre of buoyancy z_B is defined as

$$z_B = \frac{1}{V} \iiint z\, dV \tag{2.27}$$

c_{11}, c_{22}, c_{66} result from mooring arrangements and are zero in case of a free floating structure.

The oscillation of the system is considered to have built up and waves, forces and motions are approached as complex oscillations:

$$\zeta = \zeta_a \cdot e^{-i\omega t}$$
$$\underline{F_e} = \underline{F_e}^* \cdot \zeta_a \cdot e^{-i\omega t} \tag{2.28}$$

$$\underline{s} = \underline{s}^* \cdot \zeta_a \cdot e^{-i\omega t}$$

$\underline{F_e^*}$ is the vector of complex response amplification function of the excitation forces defined in its components as:

$$F_{ej}{}^*(\omega) = \frac{F_{eja}^*}{\zeta_a} \cdot e^{i\gamma_j} \quad j = 1, \dots, 6 \tag{2.29}$$

$\underline{s}^*$ is the vector of complex motion response amplification function defined in its components as

$$s_j{}^*(\omega) = \frac{s_{ja}}{\zeta_a} \cdot e^{i\epsilon_j} \quad j = 1, \dots, 6 \tag{2.30}$$

The first and second time derivatives of the position vector are then

$$\dot{\underline{s}}^* = -i \cdot \omega \cdot \underline{s}^* \cdot \zeta_a \cdot e^{-i\omega t} \tag{2.31}$$

$$\ddot{\underline{s}}^* = \omega^2 \cdot \underline{s}^* \cdot \zeta_a \cdot e^{-i\omega t} \tag{2.32}$$

The approaches of position vector (2.28) and its time derivates (2.31) and (2.32) are introduced into the initial differential motion equation (2.21). Written in its components the differential equation of motion, divided by the common factor $\zeta_a \cdot e^{-i\omega t}$ becomes:

$$\sum_{l=1}^{6} \left[-\omega^2 \cdot \left(m_{slj} + m_{hlj} \right) - i \cdot \omega \cdot b_{lj} + c_{lj} \right] \cdot s_j{}^* = F_{ej}{}^* \tag{2.33}$$

The unknown values, hydrodynamic mass, damping coefficients and excitation forces are determined by using potential flow theory (see flowing sections). The response amplification factor $H_j(\omega)$ is determined by introducing (2.30) in (2.33):

$$H_j(\omega) = \frac{s_{ja}}{\zeta_a} \cdot e^{i\epsilon_j}$$

$$= \frac{F_{ej}{}^*}{\sum_{l=1}^{6} \left[-\omega^2 \cdot \left(m_{slj} + m_{hlj} \right) - i \cdot \omega \cdot b_{lj} + c_{lj} \right]} \quad j = 1, 2, \dots, 6 \tag{2.34}$$

2.2.5 Boundary problems of a body in a wave field

The potential flow of an ideal fluid around an arbitrary floating body is limited to control volume V_C. It is confined by the sea bed S_B, the water surface S_F and the body surface S_b (Figure 10). In the xz- and xy-plane V_C is limited by S_∞ which is defined as vertical cylinder around the body and with a large radius or distance.

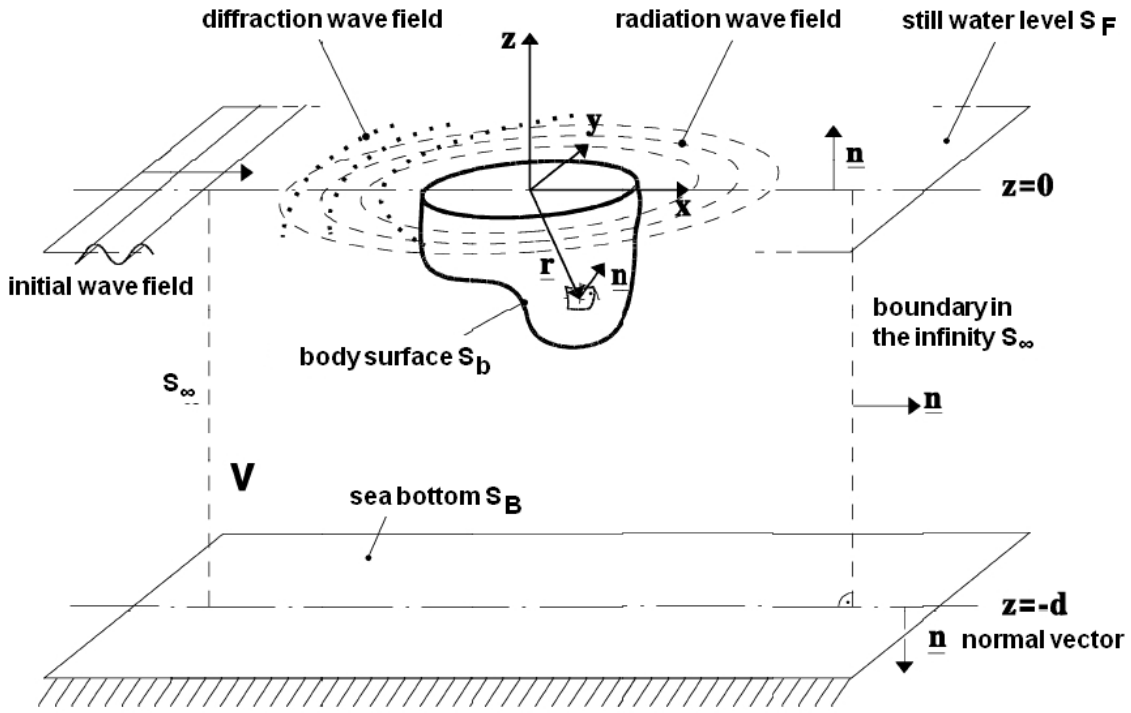

Figure 10: Schematic representation of the diffraction boundary problem of a free floating arbitrary body in waves

1. The potential flow in space V has to satisfy the Laplace equation

$$\Delta\Phi = 0 \tag{2.35}$$

following from the condition of irrotational flow and the continuity equation.

2. The linearised generalised boundary condition at the still water level S_F

$$\frac{\partial\Phi}{\partial t} + g\frac{\partial\Phi}{\partial z} = 0 \qquad \text{for } z = \zeta = 0 \tag{2.36}$$

This condition is the combination of the linearised kinematic condition and the linearised dynamic condition. The linearised kinematic condition is postulating constant pressure over the free water surface

$$\frac{\partial\zeta}{\partial t} - \frac{\partial\Phi}{\partial z} = 0 \qquad \text{for } z = \zeta = 0 \tag{2.37}$$

The linearised dynamic condition is based on the Bernoulli equation, demanding that particles do not leave the water surface

$$\frac{\partial\Phi}{\partial t} + g \cdot z = 0 \qquad \text{for } z = \zeta \tag{2.38}$$

3. The boundary condition on the sea bottom S_B, stating the particle velocity is zero

$$\frac{\partial \Phi}{\partial z} = 0 \qquad \text{for } z = -d \tag{2.39}$$

4. The boundary condition on the body surface S_b demands that no particles penetrate the body surface

$$\underline{\dot{s}}^T \cdot \underline{n} = \frac{\partial \Phi}{\partial n} \tag{2.40}$$

5. The boundary condition in infinity S_∞ or Sommerfeld's radiation condition demands that radiation waves and diffracting disturbance are travelling away from the structure.

$$\lim_{R \to \infty} \sqrt{R} \left(\frac{\partial \Phi_j}{\partial R} - ik\Phi_j \right) = 0 \tag{2.41}$$

This condition ensures that the energy of radiation and diffraction waves approximate zero with growing distance to the body.

With the assumed linearity the following approach for the total potential is made (Newmann, 1977):

$$\Phi = \Phi_0 + \sum_{l=1}^{6} \Phi_l + \Phi_7 \tag{2.42}$$

with the potential Φ_0 of the initial harmonic wave, Φ_1 to Φ_6 as the radiation potential of the 6 degrees of freedom and Φ_7 as the diffraction potential. Φ_0 is known when using for example linear wave theory. The 6 radiation potentials Φ_l are dependent on the motion of the structure. They can be divided into velocity potentials φ_l and structure velocity $\dot{s}_l$

$$\Phi_l = \dot{s}_l \cdot \varphi_l \qquad l = 1, 2, \dots, 6 \tag{2.43}$$

2.2.6 Implications of the Boundary Conditions

When the boundary condition on the body surface (2.40) is introduced into the approach of the potential Φ (2.42) we get:

$$\frac{\partial \Phi_0}{\partial n} + \sum_{l=1}^{6} \frac{\partial \Phi_l}{\partial n} + \frac{\partial \Phi_7}{\partial n} = \underline{\dot{s}}^T \cdot \underline{n} \tag{2.44}$$

and with (2.43)

$$\frac{\partial \Phi_0}{\partial n} + \sum_{l=1}^{6} \dot{s}_l \cdot \frac{\partial \varphi_l}{\partial n} + \frac{\partial \Phi_7}{\partial n} = \underline{\dot{s}}^T \cdot \underline{n} = \sum_{l=1}^{6} \dot{s}_l \cdot n_l \tag{2.45}$$

By comparing the coefficients of the above equation we get for fixed structures $\left(\underline{\dot{s}} = 0\right)$ in a wave field

$$\frac{\partial \Phi_0}{\partial n} + \frac{\partial \Phi_7}{\partial n} = 0 \tag{2.46}$$

and for a moving structure in still water

$$\frac{\partial \varphi_l}{\partial n} = n_l \qquad l = 1, 2, \ldots, 6 \tag{2.47}$$

For moving structures in a wave field both conditions apply. With (2.46) the diffraction potential can be determined by the potential of the initial wave Φ_0 and the body geometry. The function of the location of the velocity potential φ_l can be determined by (2.47) when body geometry is known.

2.2.7 Solving the boundary conditions

In order to solve the previous determined boundary conditions, with a minimum of calculation steps, a transformation into integrals becomes necessary. An approach by means of the *Second Green theorem* (Bronstein & Semendjajew, 1993) is made transforming the integral over volume to integral over a surface

$$\iiint_{V_C} [\Phi(\Delta \mathfrak{G}) - \mathfrak{G}(\Delta \Phi)]\, dV = \iint_S \left(\Phi \frac{\partial \mathfrak{G}}{\partial n} - \mathfrak{G} \frac{\partial \Phi}{\partial n}\right) dS \tag{2.48}$$

The theorem is satisfied by all the potentials of the total potential Φ. $\mathfrak{G}$ is the Green function defined as (Wehausen & Laitone, 1960):

$$\mathfrak{G}\left(\underline{x}, \underline{\xi}, t\right) = \left[\frac{1}{r} + \frac{1}{r''} + 2PV \int_0^\infty \frac{(\mu + \nu)\cosh \mu(\zeta + d)\cosh \mu(z + d)}{\mu \sinh \mu d - \nu \cosh \mu d} \mathrm{e}^{-\mu d} J_0(\mu R)\, d\mu\right] \cos(\omega t) + 2\pi \frac{k^2 - \nu^2}{(k^2 - \nu^2)d + \nu} \cosh k(z + d) \cosh k(\zeta + d)\, J_0(kR) \sin(\omega t) \tag{2.49}$$

with

$r = \sqrt{R^2 + (z-\zeta)^2}$ Distance between $\underline{x}$ and $\underline{\zeta}$

$r'' = \sqrt{R^2 + (z+2d+\zeta)^2}$ Distance between $\underline{x}$ and the reflection of $\underline{\zeta}$ at the seabed

$R = \sqrt{(x-\xi)^2 + (y-\eta)^2}$ Horizontal distance between $\underline{x}$ and $\underline{\zeta}$

$\nu = \frac{\omega^2}{g}$ Wave number for deep water

PV stands for the Cauchy principal value of the integral

$$\lim_{\varepsilon \to 0} \left[\int_0^{k-\varepsilon} f(\mu)\, d\mu + \int_{k-\varepsilon}^{\infty} f(\mu)\, d\mu \right] \tag{2.50}$$

J_0 is the Bessel function in first type and zero-order

$$J_0(x) = \sum_{k=0}^{\infty} \frac{(-1)^k \left(\frac{x}{2}\right)^{2k}}{k!\,\Gamma(k+1)} \tag{2.51}$$

The Gamma function Γ is a second order Euler integral and allows the determination of the factorial value of various numbers.

The Green function (2.49) is divided by the time harmonic function $e^{-i\omega t} \neq 0$ and introduced into the second Green function (2.48). When the boundary conditions (2.36) to (2.39) are introduced into (2.48) the surface integrals (Mei, 1989) become zero with exception of the boundary condition on the body surface S_b (2.38).[7]

$$\iint_S \dots dS = \underbrace{\iint_{S_B} \dots dS}_{=0} + \underbrace{\iint_{S_F} \dots dS}_{=0} + \underbrace{\iint_{S_\infty} \dots dS}_{=0} + \iint_{S_b} \dots dS \tag{2.52}$$

With known geometry of the body the potential Φ can be determined for every point $\underline{x} \neq \underline{\xi}$. Since $\underline{x} = \underline{\xi}$ represents a singularity the point $\underline{x}$ is surrounded by a hemisphere with the radius ε, in order to solve (2.48) at the body surface S_b. For small ε the integral (2.48) over the hemisphere $\varepsilon = \underline{x} - \underline{\xi}$ becomes $I_\varepsilon = 2\pi\Phi_j(\underline{x})$. Analogues the case of $\underline{x} \in V_C$ is solved by introducing a sphere with radius ε. In this case the integral over the sphere is $I_\varepsilon = 4\pi\Phi_j(\underline{x})$. Is $\underline{x}$ located in the body

[7] For more details see (Birk, 2001, S. 15. ff)

($\underline{x} \in E$) the integral (2.48) becomes zero since Φ and $\mathfrak{G}$ fulfil the Laplace condition.[8] For the unknown radiation and diffraction potentials ($\Phi_j,\ j = 1,\ldots,7$) we get:

$$\iiint_{V_C} \left[\Phi_j\left(\underline{\xi}\right)\left(\Delta\mathfrak{G}\left(\underline{x},\underline{\xi}\right)\right) - \mathfrak{G}\left(\underline{x},\underline{\xi}\right)\left(\Delta\Phi_j\left(\underline{\xi}\right)\right)\right] dV = 0 \tag{2.53}$$

$$0 = \iint_{S_b}\left[\Phi_j\left(\underline{\xi}\right)\frac{\partial\mathfrak{G}\left(\underline{x},\underline{\xi}\right)}{\partial n} - \mathfrak{G}\left(\underline{x},\underline{\xi}\right)\frac{\partial\Phi_j\left(\underline{\xi}\right)}{\partial n}\right] dS + \begin{cases} 0 \ \text{für}\ \underline{x} \in E \\ 2\pi\Phi_j(\underline{x}) \ \text{für}\ \underline{x} \in S_b \\ 4\pi\Phi_j(\underline{x}) \ \text{für}\ \underline{x} \in V_C \end{cases} \tag{2.54}$$

The source point $\underline{\xi}$ is always located on the body surface S_b and E is the space inside the body.

2.2.8 Radiation Potential

The equation (2.54) modified for the radiation potential

$$2\pi\underbrace{\Phi_l(\underline{x})}_{=\dot{s}_l\varphi_l} + \iint_{S_b}\underbrace{\Phi_l\left(\underline{\xi}\right)}_{=\dot{s}_l\varphi_l}\frac{\partial\mathfrak{G}\left(\underline{x},\underline{\xi}\right)}{\partial n}dS = \iint_{S_b}\mathfrak{G}\left(\underline{x},\underline{\xi}\right)\underbrace{\frac{\partial\Phi_l\left(\underline{\xi}\right)}{\partial n}}_{=\dot{s}_l\varphi_l}dS \quad l = 1,2,\ldots,6 \tag{2.55}$$

is again modified by introducing the approach of the radiation potential (2.54) an its normal derivative (2.47)

$$2\pi\varphi_l(\underline{x}) + \iint_{S_b}\varphi_l\left(\underline{\xi}\right)\frac{\partial\mathfrak{G}\left(\underline{x},\underline{\xi}\right)}{\partial n}dS = \iint_{S_b} n_l\left(\underline{\xi}\right)\mathfrak{G}\left(\underline{x},\underline{\xi}\right)dS \quad l = 1,2,\ldots,6 \tag{2.56}$$

2.2.9 Diffraction Potential

Analogous to the radiation potential the equation (2.54) is modified for the diffraction potential $\Phi_7\left(\underline{x},\underline{\xi} \in S_b\right)$

$$2\pi\Phi_7(\underline{x}) + \iint_{S_b}\Phi_7\left(\underline{\xi}\right)\frac{\partial\mathfrak{G}\left(\underline{x},\underline{\xi}\right)}{\partial n}dS = \iint_{S_b}\mathfrak{G}\left(\underline{x},\underline{\xi}\right)\underbrace{\frac{\partial\Phi_7\left(\underline{\xi}\right)}{\partial n}}_{=\frac{\partial\Phi_0}{\partial n}}dS \tag{2.57}$$

To determine the diffraction potential we approach the body surface as stream surface. The space inside the body V', which is limited by the still water S_F and the body surface S_b, is considered as part of the fluid space.

The same approach as in (2.54) is made for the potential Φ_0 of the initial wave field and we get

[8] For more details see (Birk, 2001, S. 18. ff)

$$0 = -\iint_{S_b}\left[\Phi_0\frac{\partial \mathfrak{G}}{\partial n} - \mathfrak{G}\frac{\partial \Phi_0}{\partial n}\right]dS + \begin{cases} 0 \ for\ \underline{x} \in E \\ 2\pi\Phi_0(\underline{x})\ for\ \underline{x} \in S_b \\ 4\pi\Phi_0(\underline{x})\ for\ \underline{x} \in V' \end{cases} \tag{2.58}$$

For $\underline{x} \in S_b$, if enhanced by $4\pi\Phi_0(\underline{x})$, we get

$$2\pi\Phi_0(\underline{x}) + \iint_{S_b}\Phi_0\left(\underline{\xi}\right)\frac{\partial \mathfrak{G}\left(\underline{x},\underline{\xi}\right)}{\partial n}dS = \iint_{S_b}\frac{\partial \Phi_0\left(\underline{\xi}\right)}{\partial n}\mathfrak{G}\left(\underline{x},\underline{\xi}\right)dS + 4\pi\Phi_0(\underline{x}) \tag{2.59}$$

By addition of (2.59) and (2.57), both contain integrals over S_b, we get (Lee, 1995)

$$\begin{aligned} &2\pi\Phi_D(\underline{x}) + \iint_{S_b}\Phi_D\left(\underline{\xi}\right)\frac{\partial \mathfrak{G}\left(\underline{x},\underline{\xi}\right)}{\partial n}dS \\ &\qquad = \iint_{S_b}\underbrace{\left(\frac{\partial \Phi_0\left(\underline{\xi}\right)}{\partial n} + \frac{\partial \Phi_7\left(\underline{\xi}\right)}{\partial n}\right)}_{=0}\mathfrak{G}\left(\underline{x},\underline{\xi}\right)dS + 4\pi\Phi_0(\underline{x}) \end{aligned} \tag{2.60}$$

with the total diffraction potential $\Phi_D = \Phi_0 + \Phi_7$. The integral on the right side of the equation above becomes zero since equation (2.46) is applies.

2.3 AQWA Characteristics

In this section the methods of how ANSYS AQWA calculates forces and motions of structures in waves are described. Analyses in frequency and time domain are possible. A significant advantage is the use of up to four-fold symmetry when modelling a body. The computing time saved lies between 75% and 90% when four-fold symmetry is applied.

In AQWA the storage of calculated data in backing files allows a faster workflow. This way different types of analyses can be done with the same model e.g. two backing files are created when AQWA LINE is used for a motion analysis in the frequency domain. One contains the hydrodynamic database and the other all modelling information relating to the body or bodies being analysed. Both files can be used by AQWA NAUT to conduct a motion analysis in time domain.

In addition, efficiency is increased by the implantation of restart stages. With these stages, the user is able to progress step by step to the solution of the problem, and an error made at one stage of the analysis does not necessarily mean that all the stage previous stages have to be repeated as well. The stages are:

- Stage 1 - Geometric Definition and Static Environment
- Stage 2 - Input of the Diffraction/Radiation Analysis Parameters

- Stage 3 - The Diffraction/Radiation Analysis
- Stage 4 - Input of the Analysis Environment
- Stage 5 - Motion Analysis

2.3.1 Solving Methods

For an arbitrary geometry the equations[9] (2.56) and (2.60) have to be solved numerically. The infinite number of equations has by to be reduced by dividing the structures' surface S_b into a finite number N of control points[10] $\underline{x}_i$. This discretisation is achieved by dividing the surface into N panels in the shape of squares (QPPL) and triangles (TPPL). A control point $\underline{x}_i$ is located at the centre of each panel. For each of the 6 radiations potentials Φ_l we get N equations.

$$2\pi\varphi_l(\underline{x}_i) + \sum_{k=1}^{N} \iint_{S_k} \varphi_l\left(\underline{\xi}\right) \frac{\partial \mathfrak{G}\left(\underline{x}_i, \underline{\xi}\right)}{\partial n} dS \qquad l = 1,2,\dots,6$$
$$= \sum_{k=1}^{N} \iint_{S_k} n_l\left(\underline{\xi}\right) \mathfrak{G}\left(\underline{x}_i, \underline{\xi}\right) dS \qquad i = 1,2,\dots,N \tag{2.61}$$

The diffraction potentials (2.60) become

$$2\pi\Phi_D(\underline{x}_i) + \sum_{k=1}^{N} \iint_{S_b} \Phi_D\left(\underline{\xi}\right) \frac{\partial \mathfrak{G}\left(\underline{x}_i, \underline{\xi}\right)}{\partial n} dS \qquad i = 1,2,\dots,N \tag{2.62}$$
$$= 4\pi\Phi_0(\underline{x}_i)$$

The unknown potential Φ is extracted from the integral based on the following conditions. The panel surface S_k is small enough compared to the body surface S_b so that the potential Φ is:

1. constant over the panel surfaces S_k and
2. is equal to the panel value in the control points $\underline{x}_k$.

These conditions result in the limitation on the panel geometry. In AQWA these limitations are (ANSYS, Inc., 2009b):

- Area ratio of adjacent elements < 3 with $c = 1$ for QPPL[11]

[9] 2nd order Fredholm-Integrals
[10] or collocation points
[11] Quadrilateral Pressure Plate Element

- Aspect ratio AR > 1/3 $AR = \frac{area \cdot C}{longest\ side^2}$ and $c = 2.3$ for TPPL[12]
- Panel centres at least one facet radius apart $r_f = \sqrt{area/\pi}$
- Shape factor (relation of minimum to maximum panel size) > 0.2

In AQWA the seabed S_B is implemented by mirroring the structure at the seabed. By this approach the minimum distance between floating structure and seabed limited by the facet radius r_f. Therefore must to all panels S_k be at least $r_f/2$ apart from the seabed S_B. If Φ is constant we get

$$\begin{aligned} 2\pi\varphi_l(\underline{x}_i) + \sum_{k=1}^{N} \varphi_l(\underline{x}_k) \iint_{S_k} \frac{\partial \mathfrak{G}\left(\underline{x}_i, \underline{\xi}\right)}{\partial n} dS \qquad & l = 1,2,\dots,6 \\ = \sum_{k=1}^{N} n_l(\underline{x}_k) \iint_{S_k} \mathfrak{G}\left(\underline{x}_i, \underline{\xi}\right) dS \qquad & i = 1,2,\dots,N \end{aligned} \tag{2.63}$$

and

$$2\pi\Phi_D(\underline{x}_i) + \sum_{k=1}^{N} \Phi_D(\underline{x}_k) \iint_{S_b} \frac{\partial \mathfrak{G}\left(\underline{x}_i, \underline{\xi}\right)}{\partial n} dS = 4\pi\Phi_0(\underline{x}_i) \qquad i = 1,2,\dots,N \tag{2.64}$$

2.3.2 Excitation Forces, Potential Damping and Hydrodynamic Mass

The Froude-Krylov force F_k is defined as the dynamic pressure over the body surface

$$F_k = -\iint_{S_b} p n_k \, dS \tag{2.65}$$

The dynamic pressure is determined by the linearised Bernoulli equation

$$p = -\rho \cdot \frac{\partial \Phi}{\partial t} = -\rho \left[\frac{\partial \Phi_0}{\partial t} + \sum_{l=1}^{6} \ddot{s}_l \varphi_l + \frac{\partial \Phi_7}{\partial t} \right] \tag{2.66}$$

where (2.43) is used for rearrangement of the equation. The excitation forces in the differential motion equation consist of the amount of pressure from initial and diffraction potential.

[12] Triangular Pressure Plate Element

$$F_k = \rho \iint_{S_b} \frac{\partial \Phi_D}{\partial t} n_k \, dS \tag{2.67}$$

The amplification operator of the excitation forces in relation to ζ_a is

$$F_k^* = -\frac{i\omega\rho}{\zeta_a} \iint_{S_b} \varphi_D n_k \, dS \tag{2.68}$$

The matrix of the hydrodynamic mass $\mathrm{M_h} = \{\mathrm{m_{hlj}}\}$ and potential damping $\mathrm{B} = \{\mathrm{b_{lj}}\}$ follow from

$$\mathrm{m_{hlj}} + \frac{i}{\omega}\mathrm{b_{lj}} = \rho \iint_{S_b} n_l \varphi_l \, dS \tag{2.69}$$

With the determined hydrodynamic mass matrix $\mathrm{M_h}$ and damping matrix B the response amplification factor $H(\omega)$ is calculated by

$$\begin{aligned} H_{lj}(\omega) &= \frac{s_{ja}}{\zeta_a} \cdot e^{i\epsilon_j} \\ &= \frac{\underline{\mathrm{F}}_{\mathrm{ej}}^*}{\sum_{\mathrm{l}=1}^{6}\left[-\omega^2 \cdot \left(\mathrm{m_{slj}} + \mathrm{m_{hlj}}\right) - \mathrm{i} \cdot \omega \cdot \mathrm{b_{lj}} + \mathrm{c_{lj}}\right]} \end{aligned} \qquad \mathrm{j} = 1, \ldots, 6 \tag{2.70}$$

2.3.3 Mean Wave Drift Forces (Far Field Solution)

The mean wave drift forces on a floating body in the horizontal plane may be calculated by considering the rate of change of linear and angular momentum within a prescribed fluid domain. This is known as the far field solution (Newman J. , 1967). Based on the calculated total potential Φ AQWA LINE is able to determine the mean wave drift forces as far field solution (ANSYS, Inc., 2009e). For a free floating vertical cylinder the following applies:

- The mean drift moment in yaw (about z axis) is zero. It is therefore not considered in this section.
- The magnitude of the translational mean drift force is independent of the angle of encounter and is oriented in direction of wave propagation. For that reason mean drift force is only described in x-Direction.

The rate of change of linear momentum may be written as:

$$\frac{d\underline{P}}{dt} = -\rho \int_{S_B+S_F+S_b+S_\infty} \left[\left(\frac{p}{\rho} + gz\right)\underline{n} + \underline{v}(v_n - u_n)\right] \mathrm{dS} \tag{2.71}$$

In case the body has zero forward speed and by considering the force in the horizontal plane, we have:

$$F_{DriftX} = -\int_{S_\infty} (pn_1 + \rho v_x v_n) dS - \frac{dP_x}{dt} \tag{2.72}$$

In order to obtain the mean force a time average of the above equation is determined. The last term in the equations is periodic and therefore no net increase of momentum is contributed from one cycle to another. The coordinates are expressed in polar form and substituted into the equation. The resulting mean force is:

$$\overline{F_{DriftX}} = -\int_{S_\infty} \overline{p\, sin\, \psi + \rho v_R \left(v_R \cos\psi - v_\psi \cos\psi\right) r}\, \mathrm{d}\psi dr \tag{2.73}$$

The equation is exact since no assumptions of linearity have been made. With the assumption of a small wave slope we obtain the contribution to the force which is proportional to the incident wave amplitude squared. The required potential describing the fluid field needs only to be of first order as the second order potential makes no contribution to the mean wave drift in the horizontal plane. The first order potential is known from the solution of the linear diffraction/radiation problem and therefore the polar velocities may be obtained as:

$$v_r = \frac{\partial \Phi}{\partial r} \qquad \text{and} \qquad v_\psi = \frac{1}{r}\frac{\partial \Phi}{\partial \psi} \tag{2.74}$$

The pressure is obtained from Bernoulli's equation which is:

$$p = -\rho \frac{\partial \Phi}{\partial t} - \frac{1}{2}\rho \left|\underline{v}\right|^2 - \rho g z \tag{2.75}$$

2.3.4 Significant and Maximum Motion in AQWA FER

The significant motion amplitudes determined by AQWA FER are calculated with (ANSYS, Inc., 2009c)

$$s_{Sa} = \sqrt{S(\omega) \cdot |H(\omega)|^2} \qquad \text{for } H_S = 2\ m \tag{2.76}$$

The RAOs $H(\omega)$ must be previously determined by AQWA LINE. In every case AQWA FER calculates significant motions for $\zeta_{Sa} = 1\ m$ (or $H_S = 2\ m$)[13]. If a JONSWAP spectrum is applied $S(\omega)$, γ is set to 3.3. The user defines the range of wave spectra by their peak frequencies ω_P.The transition to other significant wave heights is made by

$$s_{Sa}(H_S) = s_{Sa}\frac{H_S}{2} \tag{2.77}$$

The maximum motion amplitude is then defined by

[13] For linear wave theory

$$s_{MAXa} = \left(\frac{H_{max}}{H_s}\right)_{mode} \cdot s_{Sa}(H_S) \tag{2.78}$$

The most probable maximum wave height H_{max}, based on the Rayleigh distribution of the wave spectra, is determined by (Goda, 2000)

$$\left(\frac{H_{max}}{H_s}\right)_{mode} \simeq 0.706\sqrt{\ln N_W} \tag{2.79}$$

with the number of waves N_W in a wave train or wave record. For $N_W = 1000$, equivalent to a 3 hour storm with a peak frequency of 10 s, the most probable maximum wave height is $H_{max} = 1.86 \cdot H_s$.

2.3.5 Wind and Current

Wind and current drag are both calculated from a set of user-defined environmental load coefficients. Since the relative velocity between structure and current or wind determines drag forces and moments the hull drag coefficients must be entered even when current or wind are set to zero in the analysis. The input coefficients are defined translational as (ANSYS, Inc., 2009f)

$$\frac{F_{Drag}}{v_c^2} = 0.5 \cdot \rho \cdot A_S \cdot c_D \cdot \cos(\psi) \tag{2.80}$$

and rotational as

$$\frac{M_{Drag}}{v_c^2} = 0.5 \cdot \rho \cdot A_S \cdot c_D \cdot \cos(\psi) \cdot z_{CUR} \tag{2.81}$$

with the vertical lever of the drag force z_{CUR} in respect to COG, the projected area below water level A_S, and ψ as the angle of encounter. A velocity profile can be implemented in these coefficients by integration of the velocity profile over the shadow area. The drag coefficient c_D is dependent on shape of the body, its surface roughness and Reynolds number Rn. The Reynolds number gives a measure of the ratio of inertial forces to viscous forces. It is defined as:

$$Rn = \frac{vL}{\nu} \tag{2.82}$$

2.3.6 Mooring Lines

The applied mooring lines in AQWA have negligible weight and linear stiffness characteristics. The force of the mooring line P_{ML} is expressed as:

$$P_{ML} = P_0 + k_{ML} \cdot \Delta L \tag{2.83}$$

where P_0 is the force from pretention, ΔL the extension of the mooring line and k_{ML} the linear stiffness. The 3x3 stiffness matrix of the mooring lines C_{ML} at the the attachment points of the mooring line on the structure is

$$C_{ML} = \frac{k_{ML}}{L} N_l + (I - N_l) \frac{P_{ML}}{L}, \qquad N_l = \underline{l}^T \underline{l} \tag{2.84}$$

with the unit vector joining the attachment points of the mooring line $\underline{l} = (l_1, l_2, l_3)$, the 3x3 unit matrix I, stretched length of the mooring line L.

In order to translate C_{ML} from the point of definition to the COG a vector translation may be applied directly to a force and displacement:

$$C_{MLG} = \begin{bmatrix} I \\ X_{ML}^t \end{bmatrix} [C_{ML}] [I \quad X_{ML}] + \begin{bmatrix} 0 & 0 \\ 0 & P_M X_{ML}^t \end{bmatrix} \tag{2.85}$$

with

$$X_{ML} = \begin{bmatrix} 0 & z_{ML} & -y_{ML} \\ -z_{ML} & 0 & x_{ML} \\ y_{ML} & -x_{ML} & 0 \end{bmatrix}, \qquad P_M = \begin{bmatrix} 0 & P_z & -P_y \\ -P_z & 0 & P_x \\ P_y & -P_x & 0 \end{bmatrix} \tag{2.86}$$

x_{ML}, y_{ML} and z_{ML} are the coordinates of the attachment point on the structure relative to the COG. P_x, P_y and P_z are components of the tension in the mooring line at the attachment point. Mooring forces at the attachment points F_{ml} are translated into forces at the centre of gravity F_{ML} by

$$F_{ML} = \begin{bmatrix} I \\ X_{ML}^t \end{bmatrix} [F_{ml}] \tag{2.87}$$

2.3.7 Equilibrium with AQWA LIBRIUM

To determine an equilibrium position of a free floating or moored structure AQWA LIBRIUM is used. In the equilibrium analysis the program includes forces and moments originating from hydrostatic pressures, weights of the structures, mooring tensions, wind drag, current drag and steady wave drift forces (ANSYS, Inc., 2009d).

Hydrostatic forces and moments are determined directly from the integral of hydrostatic pressure on all the submerged elements. This is done analogous to (2.25). As the body is moved towards equilibrium, the hydrostatics are recalculated at each iteration based on the new submerged volume.

Mean drift forces are calculated with the in AQWA LINE determined mean drift coefficients $D(\omega)$ and the wave energy spectrum $S(\omega)$ as follows

$$F_D = \int_0^\infty D(\omega) S(\omega) \, d\omega \tag{2.88}$$

The wind and current drag forces and moments are calculated from the lead coefficients determined in 2.3.5. The drag coefficients for any heading are obtained by linear interpolation. The impact of mooring lines on the equilibrium is determined by the methods discussed in 2.3.6.

2.3.8 Time Domain Analysis in AQWA NAUT

AQWA NAUT is a time domain program which simulates the motions of floating structures in response to regular or irregular seas and steady wind and currents. At each time step they determine the instantaneous value of all considered forces $F(t)$ on a structure in a wave field. With (2.89) the resulting accelerations are calculated. The position and velocity are determined at the subsequent time step. This is done by integrating the accelerations in the time domain using a two stage predictor-corrector numerical integration scheme[14]. The process is then repeated in the following time step thus producing a time history of the structures motion. In order to begin the integration and prevent transients the initial condition is required. This initial condition is determined by means of AQWA LIBRIUM. (ANSYS, Inc., 2009f).

$$(M_s + M_h) \cdot \underline{\ddot{s}} = F(t) \tag{2.89}$$

The time step calculations are conducted based on the in AQWA LINE determined hydrodynamic data of the structure. They are entered via a backing file (HYD-file). At spectrum frequencies which are outside entered hydrodynamic parameters the program will automatically extrapolate the required data. At frequencies higher than those given by the backing file, the values at the highest frequency are used. At frequencies lower than those determined for analysis, a linear interpolation of the added mass and damping at the lowest frequency are used when appropriate. Wave frequency forces of diffraction and Froude Krylov are assumed to tend to zero at the low frequency range of the spectrum (ANSYS, Inc., 2009a).

All position related quantities (e.g. panels, forces) are specified with respect to a set of axes whose origin is located always at the COG of the moving body, while the axes remain parallel to the FRA (fixed reference axes) at all times. FRA is located on the free surface and Z points vertically upwards.

The program is capable of calculating the non-linear hydrostatic and Froude-Krylov wave forces of the meshed model with respect to COG. These forces are re-calculated at each time step based on all panels which make up the submerged part body. The hydrostatic force and moment at any instant in time are as follows (ANSYS, Inc., 2009f):

$$F_B(t) = -\int_{S_b(t)} p_{stat} \cdot \underline{n}\, ds \tag{2.90}$$

$$\mathrm{M_R}(t) = -\int_{S_b(t)} p_{stat} \cdot (\underline{x_i} \times \underline{n})\, ds \tag{2.91}$$

where $\underline{x_i}$ is the position vector of the panels with regard to COG, $p_{stat}(= \rho g z)$ is the hydrostatic pressure, $\underline{n}$ is the outward normal vector of the body surface and $S_b(t)$ is the wetted surface of the body at an instant in time.

[14] 2 stage implicit (semi-implicit for the non-linear drag term) predictor-corrector scheme based on the Newmark-Beta method which has proved to be highly stable (ANSYS, Inc., 2009a).

The Froude-Krylov wave forces and moments are calculated at each time step by integrating the dynamic pressure acting on each submerged panel based on the new structure position. The program offers linear and second order wave theory to calculate the Froude-Krylov wave forces. Depending on the relative water depth (d/L) AQWA NAUT applies velocity potentials for deep water or finite water depth.

$$\underline{F}(t) = -\int_{S(t)} p\underline{n}\, ds \tag{2.92}$$

The total wave forces F_e acting on a structure are the sum of the diffraction forces, calculated for regular waves by AQWA LINE, and the Froude-Krylov forces.

The structure will be subjected to the first order wave forces. The position can be determined by

$$x = H \cdot F_{wf} = \frac{F_e - M_h\ddot{x} - B\dot{x}}{C - M_S\omega^2} e^{i(kx_p - \omega t)} \tag{2.93}$$

where F_{wf} is the total wave frequency force and F_e is the complex total wave force.

In order to aid the interpretation of results the simulations are post-processed on a cycle by cycle basis, a cycle being defined as the wave period. The following information is derived from the response:

1. mean amplitude
2. fundamental wave frequency response amplitude and phase
3. harmonic components amplitude and phase
4. residual error due to transients

This is achieved by transforming the response into the frequency domain by means of the discrete Fourier transform. This allows the identification of the amplitude and phase of the fundamental wave frequency and harmonic components of the response up to the Nyquist frequency or folding frequency (half the sampling frequency).

$$s(f_k) = \frac{2\pi}{\omega} \sum_{j=0}^{N-1} s_0(j) e^{-i2\pi j \frac{k_H}{N_S}} \tag{2.94}$$

$$\Phi(f_k) = \tan^{-1}\left\{\frac{Re[s(f_k)]}{Im[s(f_k)]}\right\} \tag{2.95}$$

where $s_0(j)$ is the original response time history at time step j. The factor f_k is calculated by

$$f_k = \frac{k_H \omega}{2\pi N_S} \tag{2.96}$$

where N_S as the number of samples in a cycle and k_H as the harmonic component (i.e. 0 = mean, 1 = fundamental, 2 = second harmonic, etc.).

2.3.9 Wave Spectrum

Irregular seas are specification by input of wave spectra. Because of the manner in which the drift force is calculated, the spectrum has to be defined such that the spectral area $m(\Delta\omega) = S(\omega)\Delta\omega$ between adjacent spectral lines ω_n is equal (ANSYS, Inc., 2009f).

$$\int_{n=i}^{i+1} S(\omega_n)\, d\omega = \int_{n=i+1}^{i+1} S(\omega_n)\, d\omega, \quad i = 1, 2, \ldots \tag{2.97}$$

The program does this by calculating the spectral density by default at 5000 raster points on the frequency scale, which are equally spaced between the defined spectrum end frequencies. The raster is then divided into the required number of spectral 'packets' such that the spectral area of each packet satisfies (2.97). Linear interpolation is used between the raster points to help define the limits of the packets. A spectral line is then defined at the frequency at the centre of area of the packet $(\omega_i + \omega_{i+1})/2 = \omega_m$. This is equivalent to the first moment of area of the spectral energy m_1 becoming zero.

$$m_1 = \int_{n=i}^{i+1} S(\omega_n)\omega_n\, d\omega = 0, \qquad i = 1, 2, \ldots \tag{2.98}$$

2.3.10 Limitations of Theoretical Applications

The main theoretical limitations of AQWA LINE are listed below:

1. The theory relates to a body or bodies which have zero or small forward speed (with impact on AQWA NAUT)
2. If first order rigid body motions are required, then the mean body position must be one of static equilibrium.
3. The motions are to a first order and hence must be of small amplitude (with impact on AQWA NAUT)
4. The incident regular wave train must be of small amplitude compared to its length (i.e. small slope).
5. The fluid is assumed inviscous, incompressible and the fluid flow irrotational. (with impact on AQWA NAUT)
6. All body motions are harmonic.
7. Viscous effects like viscous roll damping are not included within the analysis. Viscous damping must be added manually.

The main theoretical limitations of AQWA LIBRIUM are listed below:

1. Stability information is only valid for small displacements about the equilibrium position.

The main theoretical limitations of AQWA NAUT are listed below:

1. The diffraction and radiation parameters are calculated by AQWA LINE (linear theory), therefore all terms such as diffraction force, added mass and radiation damping are linear quantities.

3 Results

The hydrostatic and hydrodynamic analyses are conducted for the transit draft (T00) and a range of drafts of the lowering process (T10-T35) as seen in Figure 11. A final draft of 33 m (T33) for dynamic analyses was chosen due to limitations in AQWA regarding the distance between structure and seabed. A range of drafts is analysed to determine changes in stability and dynamic behaviour during the lowering of the structure. Due to the rotational symmetry about its z-axis the structure of the GBF is analysed by 2 dimensional considerations. Results of the free floating structure determined for sway and pitch (and trim) are also valid for surge and roll (and heel) respectively.

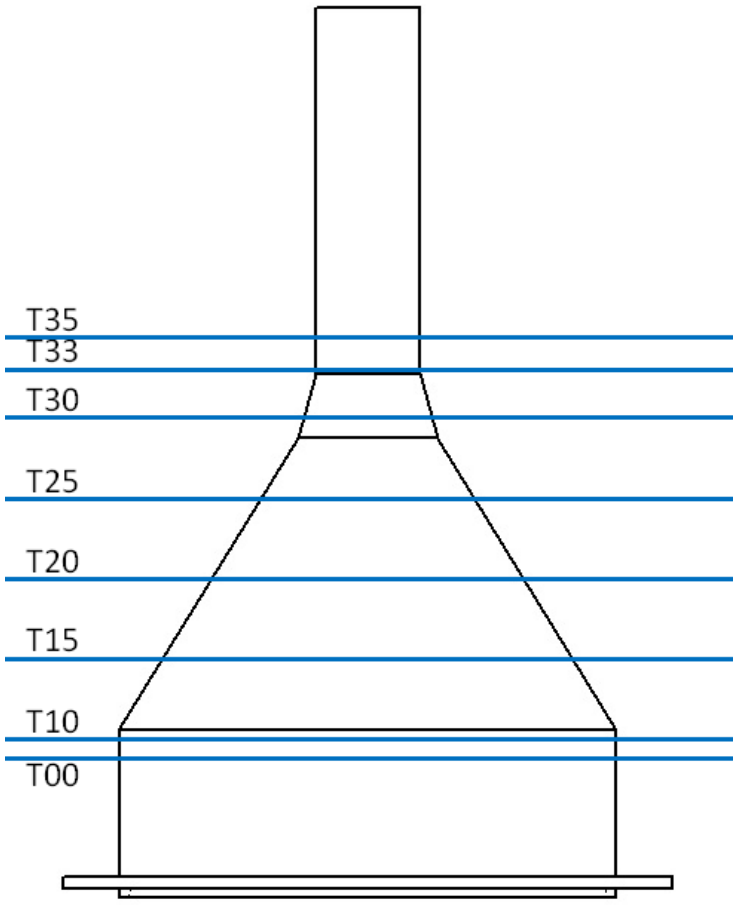

Figure 11: Analysed draft range from T00 to T35

3.1 Hydrostatic Analysis

The hydrostatic properties of the GBF at the respective drafts are listed in Table 5. It proves that the GBF is initially definite in shape, in the draft range from T00 to T15. At this stage COG is above COB. A positive initial stability $\overline{GM_0}$ is given by the sufficiently large $\overline{BM_0}$. At T15 a significant reduction of $\overline{BM_0}$ is seen, due to the immersion of the lower cone decreasing the water plane area. Additionally, the free surface moments are increased caused by the flooding of the outer tanks.

With further increase of the draft the COB shifts above the COG. In the draft range from T20 to T35 the GBF is definite in weight. The positive impact of $\overline{BM_0}$ on the initial stability becomes negligibly small. When the ballast water in the tanks overflows at T35 a significant increase of free surface moments is seen.

	T00	T10	T15	T20	T25	T30	T33	T35
Draft T [m]	8.82	10.00	15.00	20.00	25.00	30.00	33.00	35.00
Displ. [t]	6962	7909	11285	13368	14465	14901	15025	15093
Ballast [t]	0.0	947.5	4323.8	6406.2	7503.6	7939.3	8063.3	8131.4
A_{WL} [m²]	779.31	779.31	522.92	299.96	138.57	49.66	31.56	33.25
$\overline{KB}$ [m]	4.48	5.07	7.24	8.80	9.82	10.32	10.50	10.60
$\overline{BM_0}$[15] [m]	7.08	6.23	1.97	0.55	0.11	0.01	0.01	0.01
FSM [m]	0.00	0.13	0.40	0.32	0.23	0.19	0.19	1.54
$\overline{KG}$ [m]	10.33	9.74	8.11	8.22	8.46	8.59	8.62	8.65
$\overline{GM_0}$ [m]	1.24	1.43	0.71	0.81	1.24	1.56	1.69	0.42
$\overline{GB}$ [m]	-5.85	-4.67	-0.86	0.58	1.36	1.74	1.87	1.96
Tank Overflow [Deg]	-	32	29	25	10	2	0	-

Table 5: Hydrostatic data of the GBF including the free surface effects of the ballast water

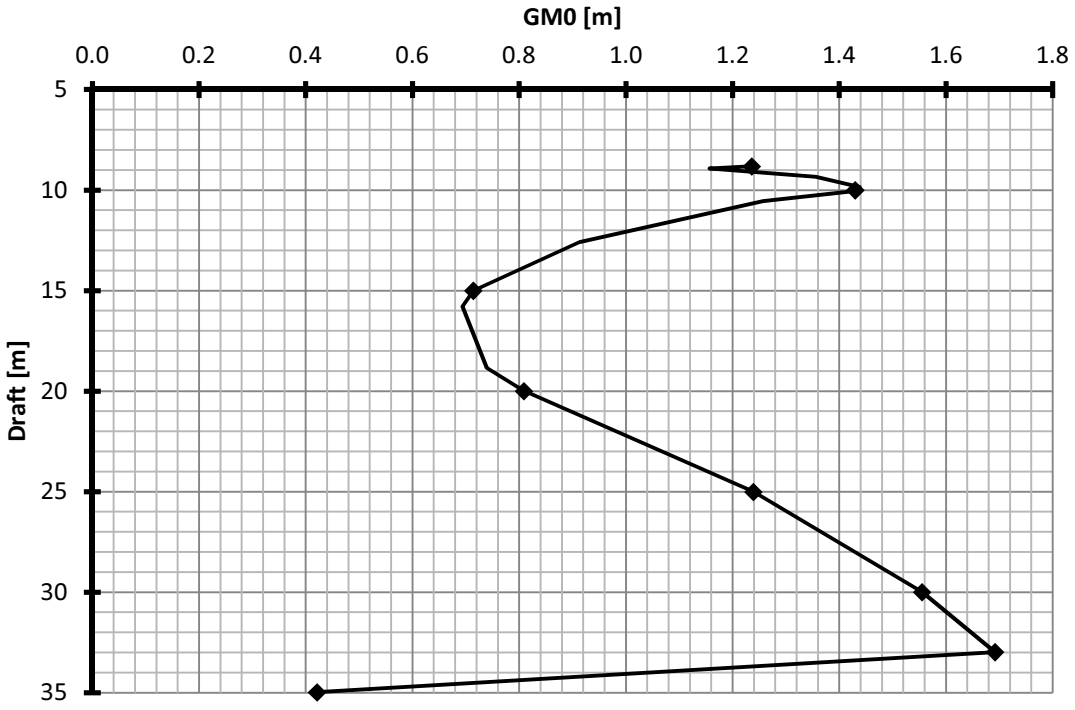

Figure 12: Initial stability $\overline{GM_0}$ in respect to draft T

[15] Without the reduction by free surface moments (FSM)

In Figure 12 initial stability $\overline{GM_0}$ is plotted in relation to draft T. Here the transition from definite in shape to definite in weight can be seen in an increase of $\overline{GM_0}$ at drafts greater than 15 m. The reduction of $\overline{GM_0}$ at transit draft as well as 10 m and 33 m draft originate from increase of free surface moments in the tanks. The first reduction of $\overline{GM_0}$ originates from the initiation of the flooding of the central tank. At 10 m draft the outer tanks are flooded. The final reduction is caused by the overflowing of the tanks walls at 33 m.

The associated righting lever curves of all drafts are plotted in Figure 13. At an angle where at least one of the tanks would overflow all tanks are considered to be linked. Ballast water shifts to the lowest point in the tanks inducing relatively large heeling moments. This can be seen in a large reduction of righting lever in the $\overline{GZ}$-curve. This approach must be considered conservative since restriction of tank walls is neglected and the full amount of ballast water is able to shift. The reduction of the righting lever decreases with increasing draft.

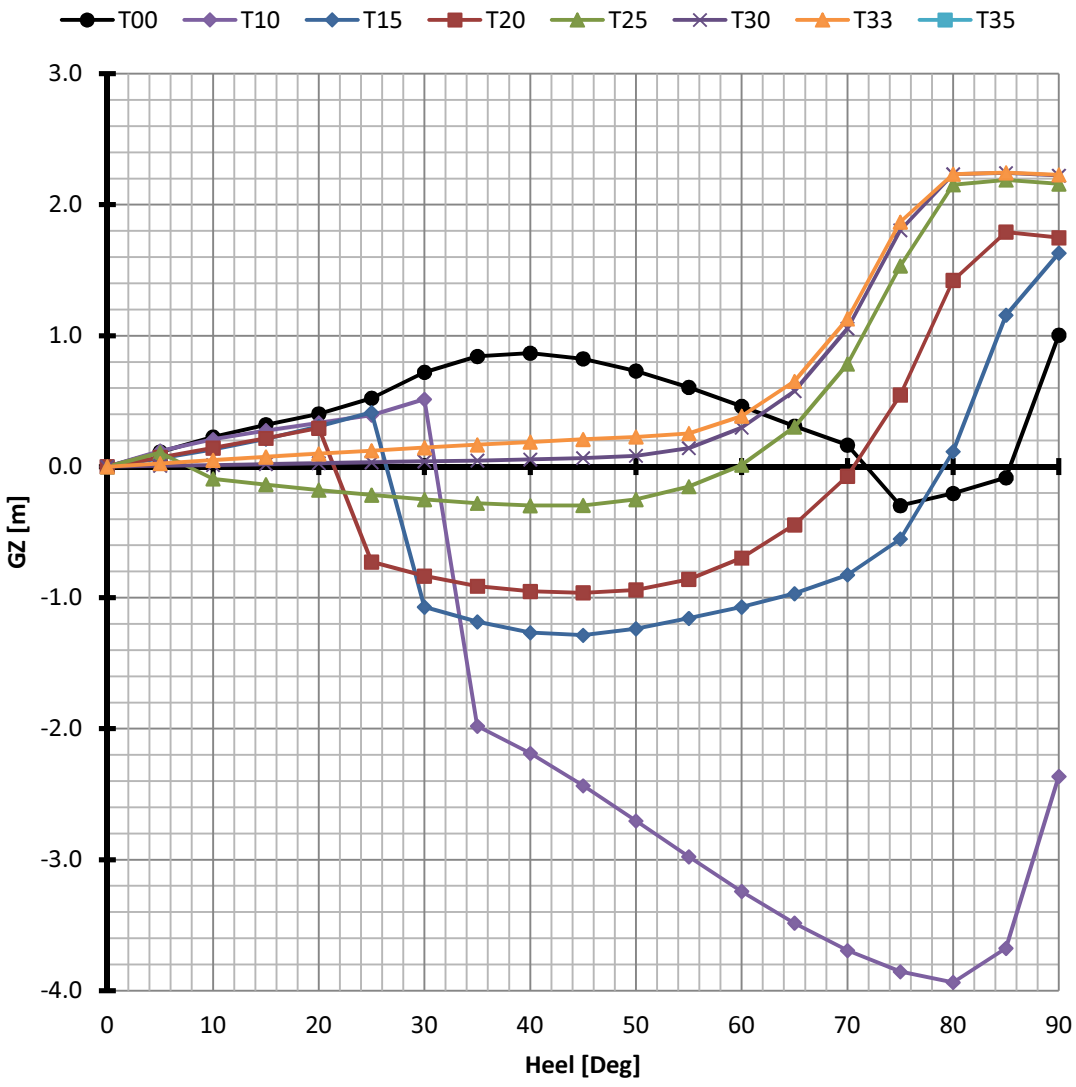

Figure 13: Righting lever curves of considered drafts from T00 to T35

3.2 Numerical Model

In this section the in AQWA generated models are checked for spatial and temporal convergence. In addition the amount of viscous damping is approximated and the impact of viscous damping alterations on the motion response is determined. Lastly, the required hull drag for time step simulations is calculated.

Figure 14: Mesh of AQWA model 100 (isometric view)

3.2.1 Spatial Convergence

A range of models has been generated with the ANSYS AQWA Workbench. The mesh characteristics are listed in Table 6. All models are corrected in regard to buoyant volume and centre of buoyancy by adding corresponding point buoyancy in the AQWA input file. Corrections are required due to the deviations from the exact geometry of the GBF generated in the meshing process. Curved surfaces are here approximated by flat panels (rectangles and triangles). The negligence of a skirt in the numerical model must also be considered.

Since x- and y-symmetry (four-fold symmetry) is applied in AQWA, in order to save computation time, the mesh data in Table 6 is given for a quarter of the total structure. The mesh is generated with regard to their maximal panel size. A panel size of 0.65 m is identified as the maximum possible resolution due to the limitation on the number of nodes in AQWA. Its model data are used as the basis for a spatial convergence test.

Model	Maximum Panel Size [m]	No. of Nodes	No. of Panels
200	2.00	1036	981
150	1.50	1796	1723
130	1.30	2409	2324
110	1.10	3265	3170
100	1.00	3840	3739
90	0.90	4802	4691
80	0.80	5961	5849
75	0.75	6761	6636
65	0.65	8984	8849
LIMIT	-	9999	18000

Table 6: Four-fold symmetry model characteristics of the spatial convergence test

Spatial convergence of the GBF model is determined by comparing RAOs calculated with AQWA in surge[16], heave and pitch. This method is chosen since added mass, potential damping and restoring coefficients, calculated by AQWA, are bases for the determination of the RAOs. Variations in the RAOs are limited to their maximum at the natural frequency of the GBF (See Figure 15 and Figure 16). Thus the deviation from the maximum of model 65 is used to qualitative convergence of the models (Table 7).

Model		**200**	**150**	**130**	**110**	**100**	**90**	**80**	**75**	**65**
Maximum Deviation	Heave	-6.1%	-4.2%	-4.8%	-3.8%	-2.8%	-2.0%	-1.4%	-0.7%	0.0%
	Pitch	9.5%	4.8%	-6.8%	-5.6%	-2.9%	-2.6%	-0.7%	0.8%	0.0%

Table 7: Deviation of RAO maximum in relation to model 65 in the spatial convergence test

All further analyses are conducted with a model 100. With this model, calculation time is reduced significantly. The tolerated deviation is relatively small (< 5%) and limited to the peak of the natural frequency. In Figure 14 the mesh of model 100 is shown.

[16] Comparison of RAOs in surge showed no significant changes in the spatial convergence test.

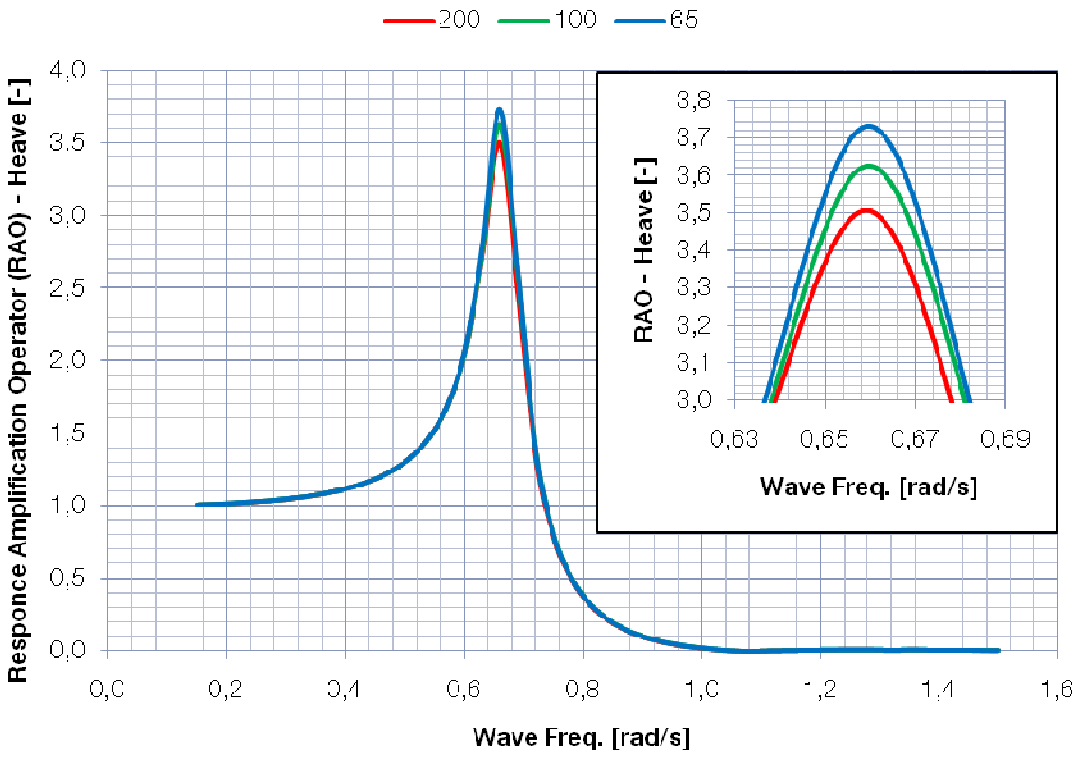

Figure 15: Spatial convergence test with ROA in heave

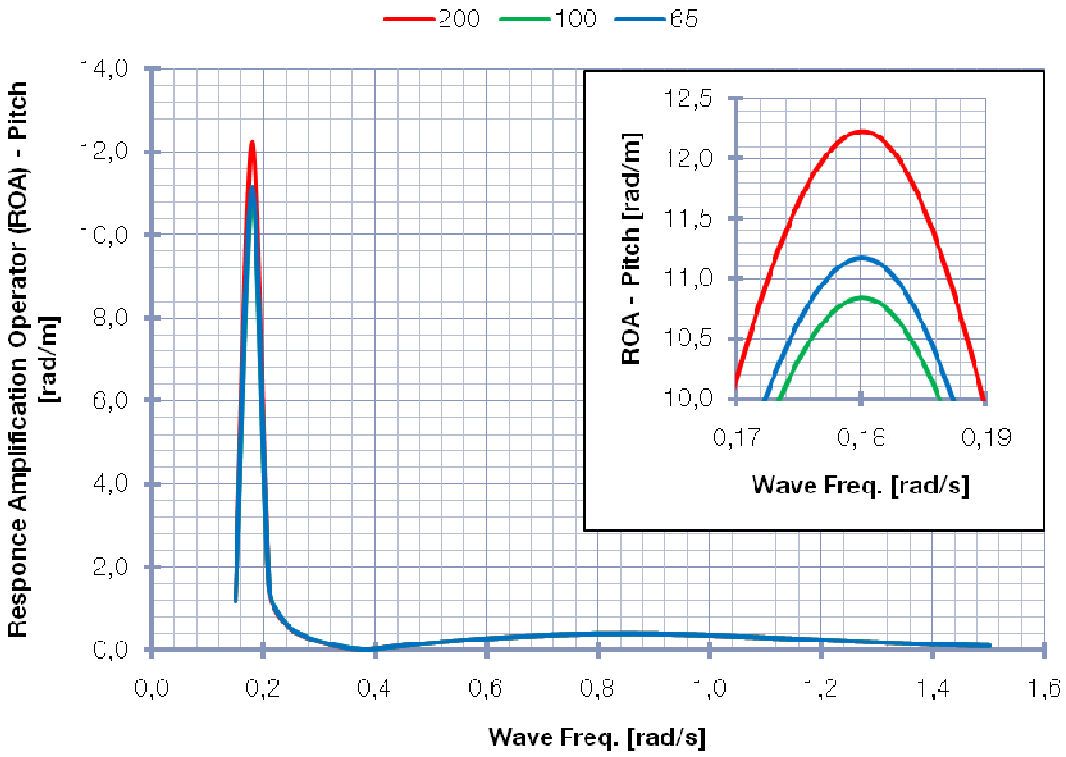

Figure 16: Spatial convergence test with ROA in pitch

3.2.2 Temporal Convergence

The previously chosen model 100 is analysed in regard to its temporal convergence. A series of time steps analyses at transit draft (T00) is conducted in AQWA NAUT. The duration of all analyses is set to 7000 seconds considering approximately 1000 waves for the applied 7 seconds peak period JONSWAP spectra and a significant wave height of 2 m. A time step of 0.005 seconds is taken as base of evaluation for the temporal convergence analyses. The range of time steps and the associated divergences of motion in percent are given in Table 8.

Time Step [s]	1.000	0.500	0.250	0.010	0.005
Max Heave Deviation	7.3%	4.8%	2.3%	0.6%	0.0%
Max Pitch Deviation	2.3%	1.8%	0.6%	0.3%	0.0%

Table 8: Comparison of motion for the temporal convergence test

In Figure 17 and Figure 18 excerpts of the time step simulation are seen, showing heave and pitch motions of COG. In heave the equilibrium position of COG is found at 1.52 m above calm water level. Divergence in amplitude and phase of the motion is reduced with decreasing time step. A time step of 0.2 seconds is used for all simulations in the time domain allowing a margin of error of less than 2.3%.

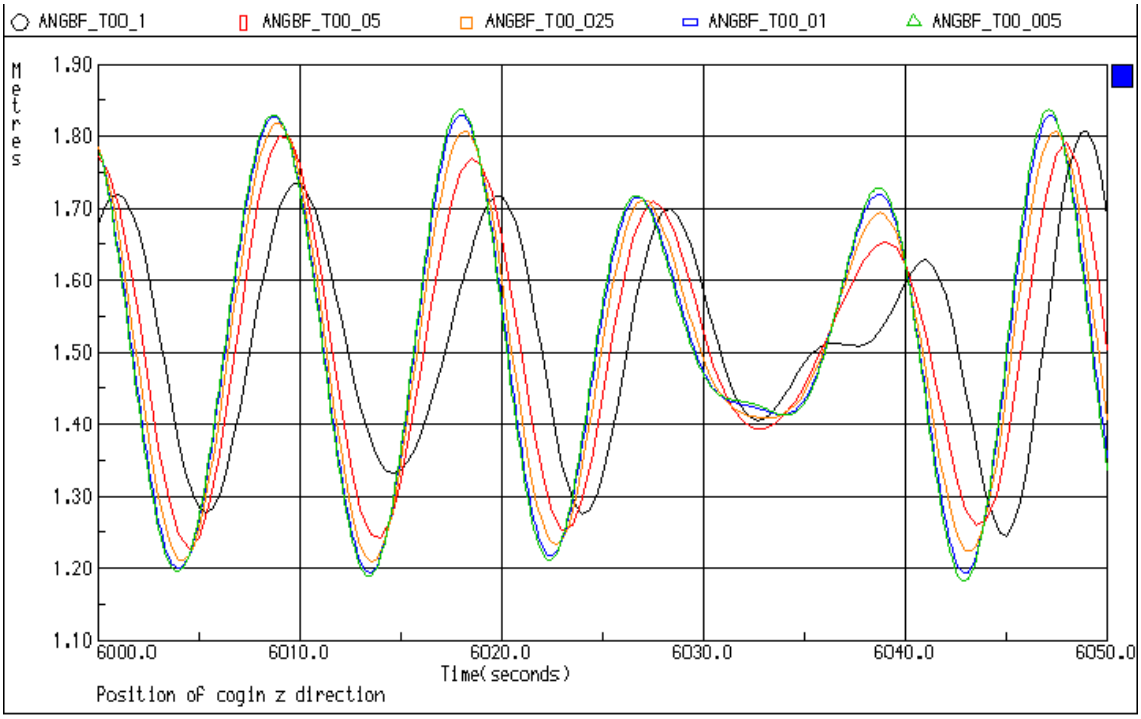

Figure 17: Temporal convergence test for heave motion (equilibrium position of COG at 1.52 m above calm water level)

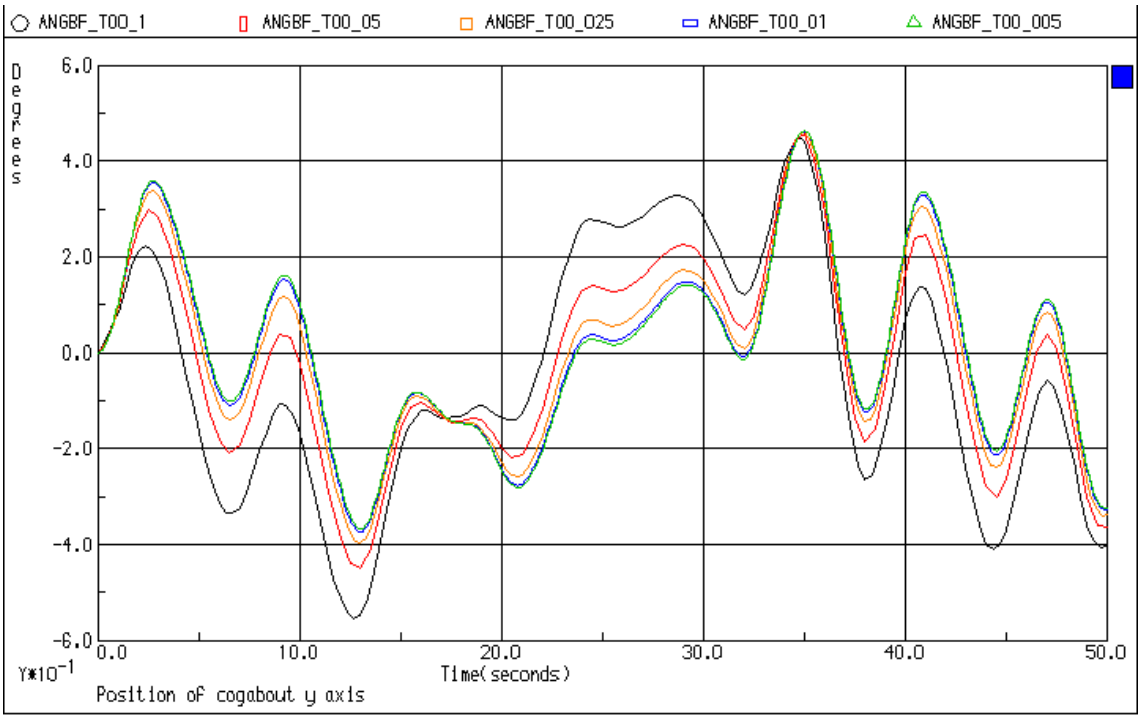

Figure 18: Temporal convergence test for pitch motion

3.2.3 Approximate Viscous Damping

The edges of the base slab promote viscous damping in heave und pitch motions. In decay tests (DHI, 2011) the damping factor k_b is determined for the drafts T00, T10 and T15. For greater drafts (T20-T33) the unknown damping factor k_b is set to the value of the draft T15 of 0.07. This is considered conservative since k_b increases with draft for the known values. In prior AQWA LINE runs, without additional viscous damping, the following values are calculated for each draft:

- restoring coefficients c
- natural frequency ω_0
- hydrodynamic mass m_h at natural frequency ω_0
- potential damping b_p at natural frequency ω_0

With known critical damping coefficient b_c

$$b_c = 2 \cdot \sqrt{c \cdot (m + m_h(\omega_0))} \tag{3.1}$$

the total damping coefficient b and viscous damping coefficient b_v are calculated by:

$$b_v = \underbrace{k_b \cdot b_c}_{b} - b_p(\omega_0) \tag{3.2}$$

Draft	Natural Frequency	Stiffness	Structural Mass	Added Mass	Damping Factor	Critical Damping Coefficient	Potential Damping Coefficient	Viscous Damping Coefficient
	ω_{R33} [rad/s]	c_{33} [kN/m]	m_{33} [t]	m_{h33} [t]	k_{b33} [-]	b_{c33} [t/s]	b_{p33} [t/s]	b_{v33} [t/s]
T00	0.67	7832	6962	10729	0.06	23541	1064	349
T10	0.65	7832	7909	10873	0.06	24257	1058	398
T15	0.46	5255	11285	13098	0.07	22640	307	1277
T20	0.32	3013	13368	15730	0.07*	18727	83	1228**
T25	0.21	1391	14465	18595	0.07*	13563	18	931**
T30	0.11	498	14901	24232	0.07*	8826	3	615**
T33	0.08	333	15025	37585	0.07*	8366	2	583**

* assumed damping factors, ** not applied added viscous damping coefficients

Table 9: Approximated viscous damping in heave

A reduction of the viscous damping coefficients in heave $\boldsymbol{b_{v33}}$ with increasing draft, as seen in Table 9, is unlikely since the wetted surface increases and therefore more frictional surface exists. Based on this assumption the added viscous damping coefficient b_{v33} will be set to 1277 t/s for the drafts T20 to T33.

Draft	Natural Frequency	Stiffness	Structural Mass	Added Mass	Damping Factor	Critical Damping	Potential Damping	Viscous Damping
	ω_{R55} [rad/s]	c_{55} [kN/m]	m_{55} [kt·m²]	m_{h55} [kt·m²]	k_{b55} [-]	b_{c55} [kt·m²/s]	b_{p55} [kt·m²/s]	b_{v55} [kt·m²/s]
T00	0.18	86.45	1932.5	798.8	0.03	971.9	0.0	29.1
T10	0.20	110.91	1961.4	764.4	0.04	1099.7	0.0	44.0
T15	0.16	79.01	2265.6	736.3	0.06	974.1	0.0	58.4
T20	0.19	106.05	2364.5	727.9	0.06*	1145.3	0.0	68.7
T25	0.23	175.75	2671.3	805.1	0.06*	1563.3	0.0	93.8
T30	0.26	227.21	2406.4	1018.7	0.06*	1764.3	0.2	105.7
T33	0.26	249.29	2409.3	1438.8	0.06*	1958.9	0.3	117.2

* assumed damping factors

Table 10: Approximated viscous damping in pitch

3.2.4 Damping Sensitivity Analysis

A damping sensitivity analysis is conducted for the model in transit draft T00. With it the impact of the added linear viscous damping on the calculated motions is specified. In the analysis the previously applied damping coefficient k_{bij} for heave and pitch motions is varied by ±0.01. The methods used to calculate the applied viscous damping coefficient b_{vij} is described in section 3.2.3.

The RAOs of the GBF for heave and pitch are determined by AQWA LINE each with reduced and increased viscous damping. The input data and the results are shown in Table 11 and Table 12. In Figure 19 and Figure 20 the associated RAOs are seen. The alteration of added linear viscous damping shows the expected magnitude variations of RAOs maxima. In the ROAS maxima of pitch motions significant deviations are seen. At the associated wave frequency total damping derives significantly from viscous damping (See Table 10). This results in a strong sensitivity towards the viscous damping alterations. In heave the impact on the ROA maxima is less significant.

Damping Case in Heave	Deviation on total Damping [%]	Damping Factor k_{b33} [-]	Viscous Damping b_{v33} [t/s]	Deviation RAO Maximum [%]
Reduced	-17	0.05	113	12
Original	±0	0.06	349	0
Increased	+17	0.07	584	-14

Table 11: Applied viscous damping coefficients and maximum resulting deviation in RAO in heave at natural frequency for damping sensitivity analysis

Damping Case in Pitch	Deviation on total Damping [%]	Damping Factor k_{b55} [-]	Viscous Damping b_{v55} [kt·m²/s]	Deviation RAO Maximum [%]
Reduced	-33	0.02	19.4	50
Original	±0	0.03	29.1	0
Increased	+33	0.04	38.9	-25

Table 12: Applied viscous damping coefficients and maximum resulting deviation of RAOs in pitch at natural frequency for damping sensitivity analysis

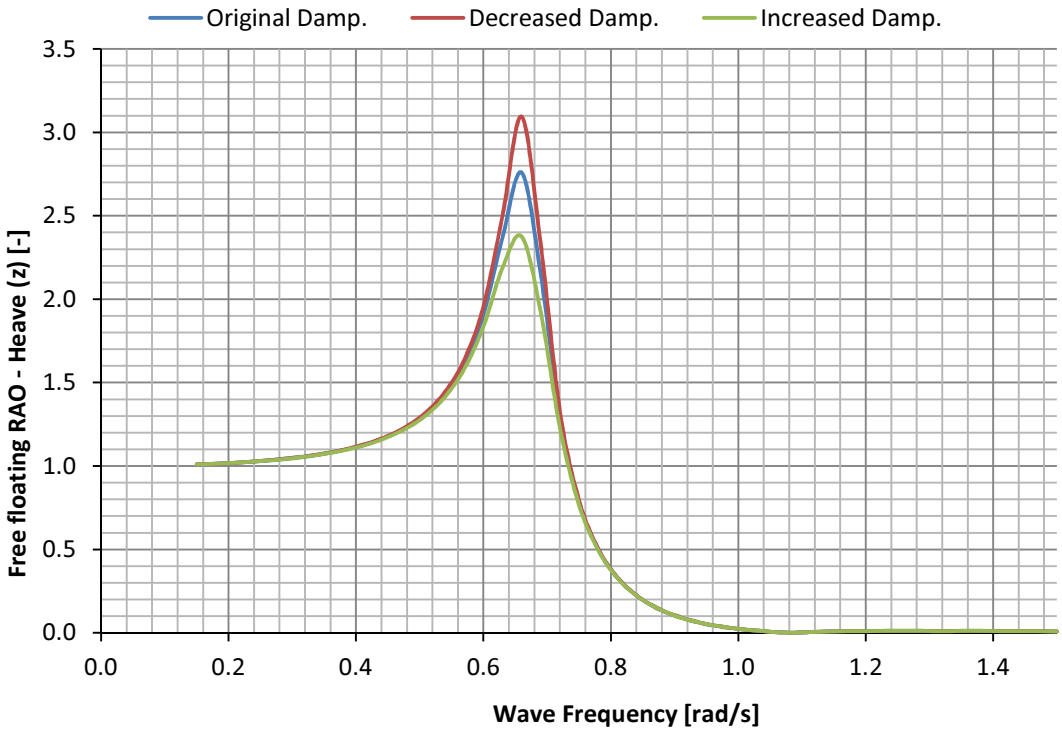

Figure 19: Damping sensitivity analysis of heave RAO

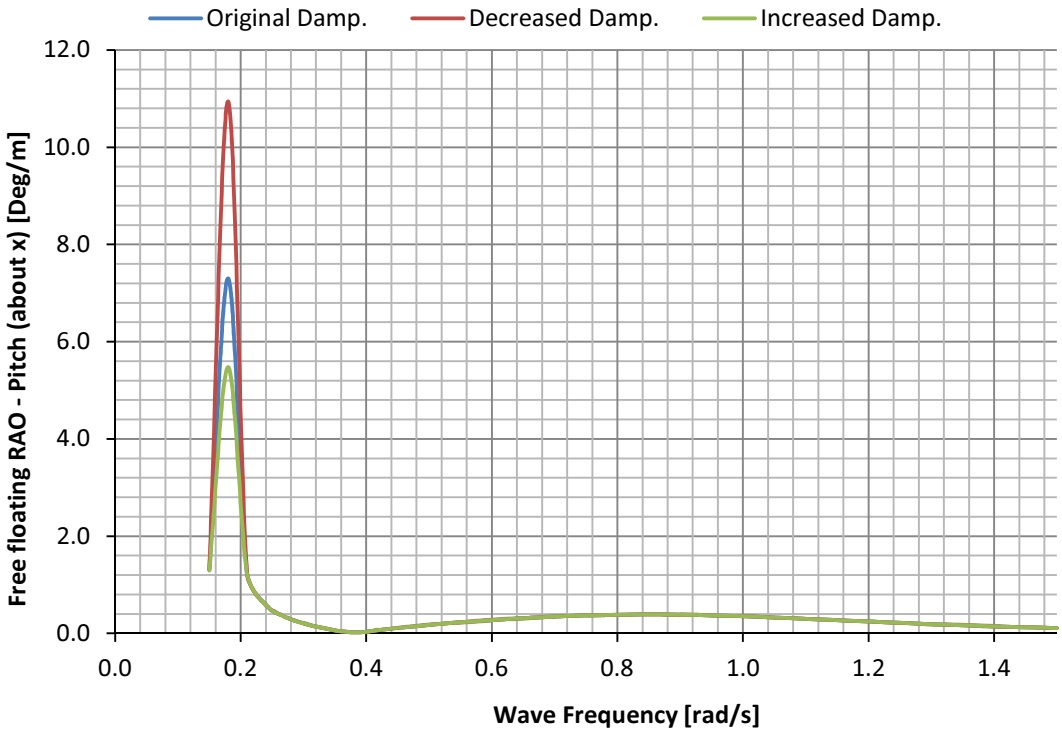

Figure 20: Damping sensitivity analysis of pitch RAO

Additionally the effects on the significant heave and pitch motions are determined by AQWA FER. The significant motions are listed and calculated for a range of JONSWAP spectra with peak frequencies from 0.42 rad/s to 1.26 rad/s (See Table 13 and Table 14). No alteration in the significant pitch motion is seen in the range of considered wave spectra. In heave the significant motions vary up to 9%

for the model with the original viscous damping. This is equivalent to a 0.07 m variation at 1m significant wave height.

Peak Frequency	Decreased Damping	Original Damping	Increased Damping
1.26	0.01	0.01	0.01
1.14	0.03	0.03	0.03
1.05	0.07	0.07	0.07
0.97	0.15	0.14	0.13
0.90	0.24	0.22	0.20
0.84	0.35	0.32	0.29
0.79	0.47	0.44	0.40
0.74	0.63	0.58	0.53
0.70	0.79	0.74	0.67
0.66	0.91	0.85	0.78
0.63	0.93	0.87	0.80
0.60	0.89	0.84	0.78
0.57	0.85	0.80	0.74
0.55	0.80	0.76	0.71
0.52	0.77	0.73	0.69
0.50	0.75	0.71	0.67
0.48	0.73	0.70	0.66
0.47	0.71	0.68	0.65
0.45	0.70	0.67	0.64
0.43	0.69	0.66	0.63
0.42	0.67	0.65	0.62

Table 13: Significant heave motions of the 3 damping sensitivity models

Peak Frequency	Decreased Damping	Original Damping	Increased Damping
1.26	0.09	0.09	0.09
1.14	0.12	0.12	0.12
1.05	0.14	0.14	0.14
0.97	0.15	0.15	0.15
0.90	0.16	0.16	0.16
0.84	0.17	0.17	0.17
0.79	0.17	0.17	0.17
0.74	0.17	0.17	0.17
0.70	0.16	0.16	0.16
0.66	0.16	0.16	0.16
0.63	0.15	0.15	0.15
0.60	0.15	0.15	0.15
0.57	0.14	0.14	0.14
0.55	0.13	0.13	0.13
0.52	0.13	0.13	0.13
0.50	0.12	0.12	0.12
0.48	0.11	0.11	0.11
0.47	0.10	0.10	0.10
0.45	0.10	0.10	0.10
0.43	0.09	0.09	0.09
0.42	0.09	0.09	0.09

Table 14: Significant pitch motions of the 3 damping sensitivity models

3.2.5 Hull Drag

The translational and rotational hull drag coefficient CUF and CUR are entered into the AQWA LIBRIUM and NAUT input file. For the calculation of the drag coefficients of the GBF, base slap is neglected and the structure is approximated by a cylinde. For Reynolds numbers Rn over $4 \cdot 10^6$ the drag coefficient C_D of a cylinder is 0.7 (Journée & Massie, 2001). This Reynolds number is equivalent to a flow of $0.13\ m/s$ around the socket with the diameter of $31.5\ m$.

Drafts	**T00**	**T15**	**T25**	**T33**
Drag Force Coefficient [kN·s²/m²]	101	167	237	263
Drag Force Coefficient about COG [kN·m·s²/m²]	-608	-141	783	911

Table 15: Drag force and moment coefficients

3.3 Motion Analysis in Frequency Domain

The RAOs (response amplification operators) of the GBF are determined by AQWA LINE. The program solves the RAOs in the frequency domain. Viscous damping is added manually to the potential damping matrix calculated by AQWA LINE as seen in section 3.2.3.

3.3.1 RAOs in Surge

The determined RAOs for pitch motion for all considered drafts are shown in Figure 21 below.

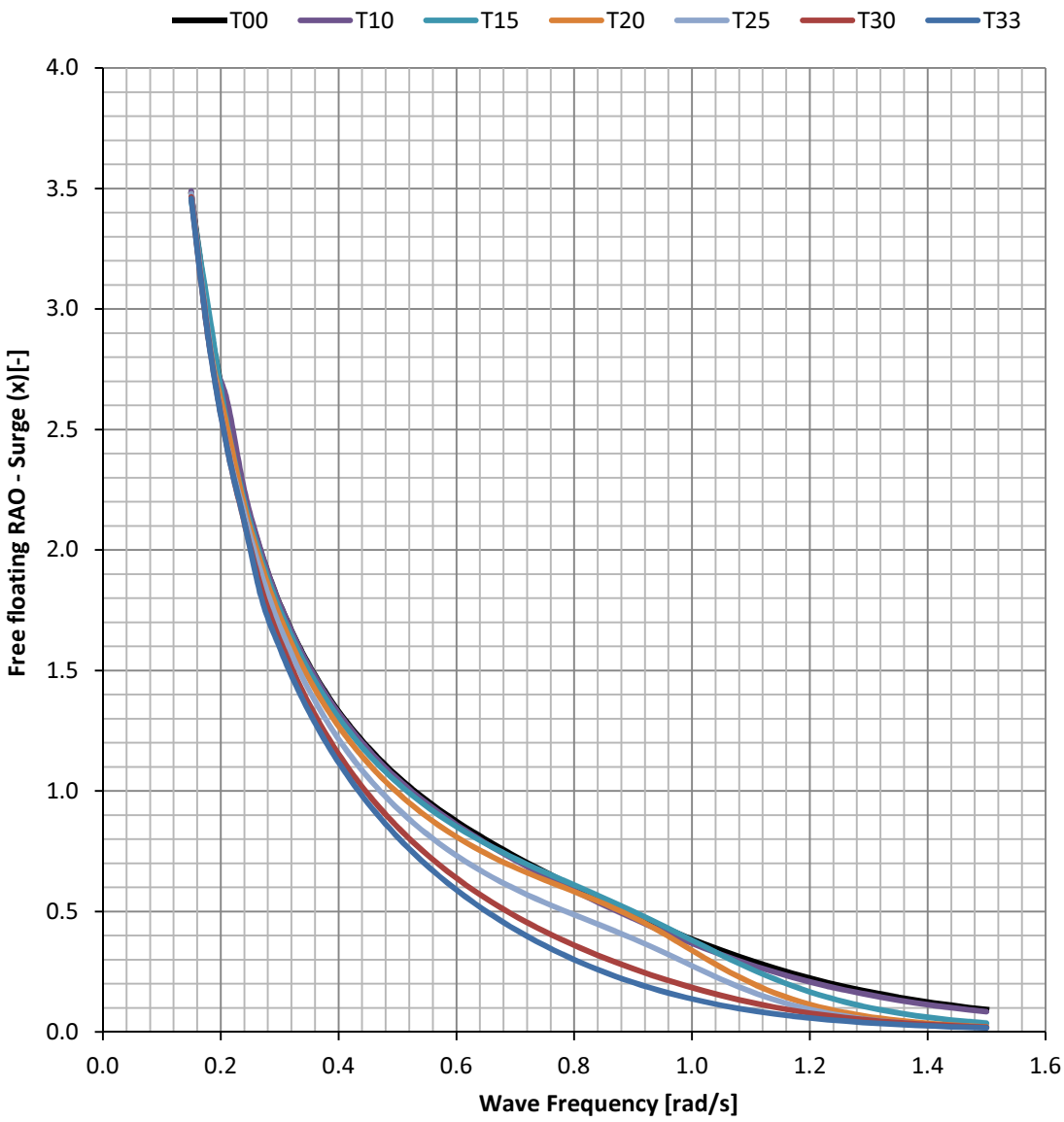

Figure 21: Free floating RAOs in surge (water depth d = 35 m)

3.3.2 RAOs in Heave

The determined RAOs for heave motion including the approximate viscous damping for all considered drafts are shown in Figure 22 below. It proves that natural frequencies are decreasing with draft. Natural frequencies show great conformity with the results from model tests. In general the determined RAO curves present the expected course at the higher and lower end of the considered frequency range. All curves show a minimum next to the natural frequency representing a cancellation frequency.

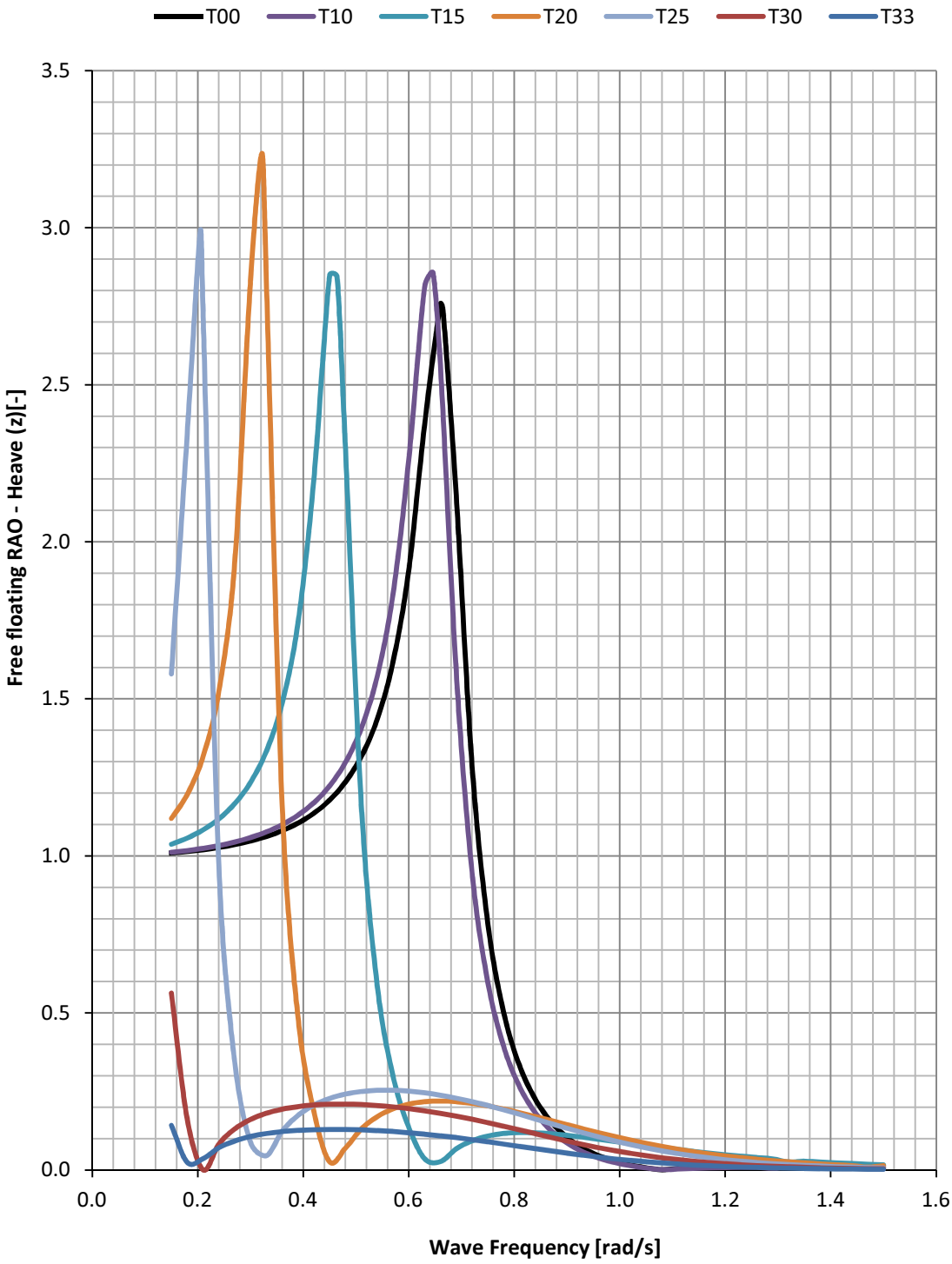

Figure 22: Free floating RAOs in heave (water depth d = 35 m)

3.3.3 RAOs in Pitch

The determined RAOs for pitch motion including the approximated viscous damping for all considered drafts are shown in Figure 23 and Figure 24 below. Natural frequencies of the RAOs in pitch are located at the lower end of the considered frequencies range. Their dependency on $\overline{GM_0}$ is seen when compared with Figure 12. Natural frequencies show good accordance with model tests as well. A resonance frequency is also seen next to the natural frequency at drafts from T00 to T20. This characteristic is not depicted at greater drafts due to the larger damping. At the higher and lower end of the considered frequency range the determined RAO curves present the expected course.

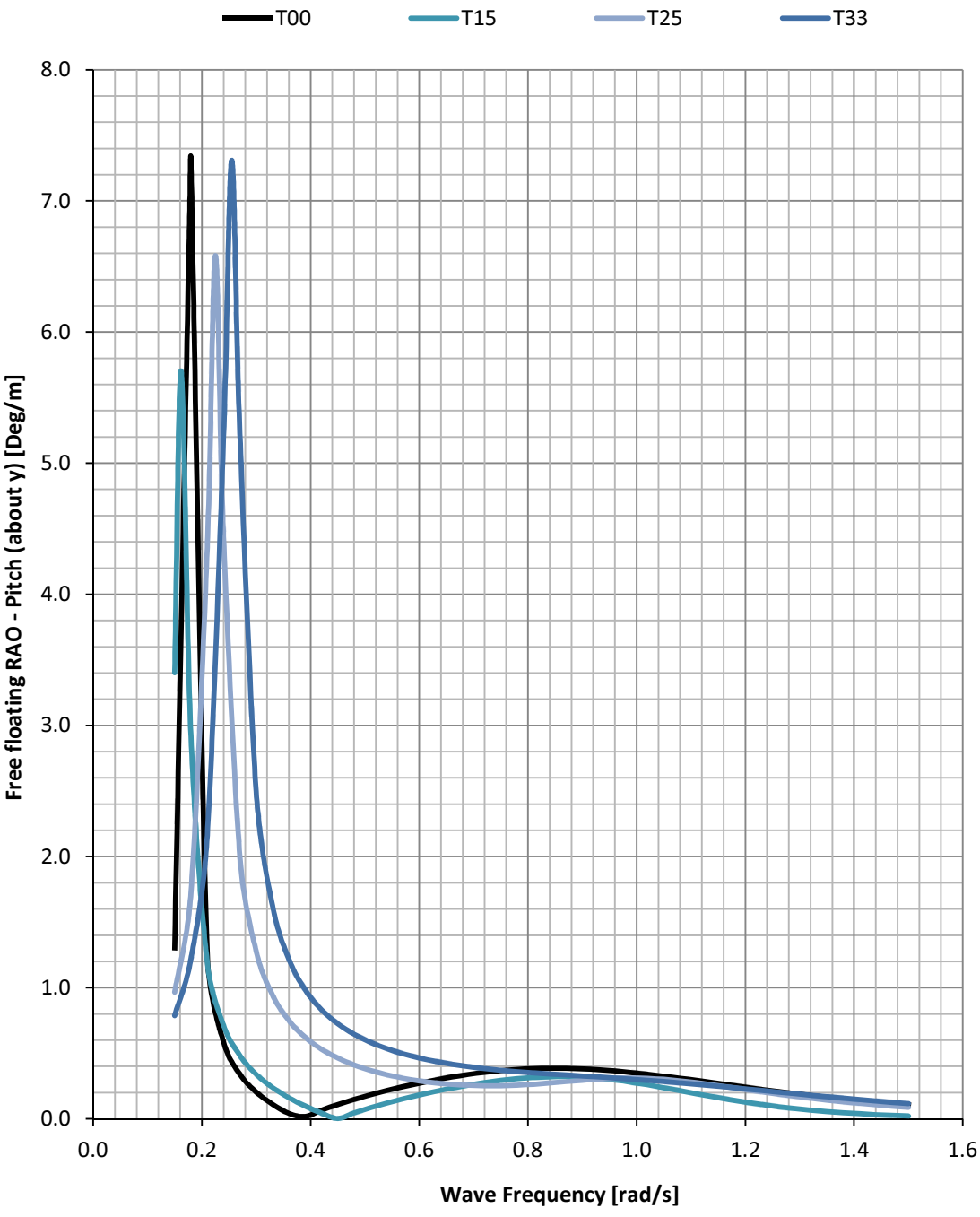

Figure 23: Free floating RAOs in pitch for T00, T15, T25 and T33 (water depth d = 35 m)

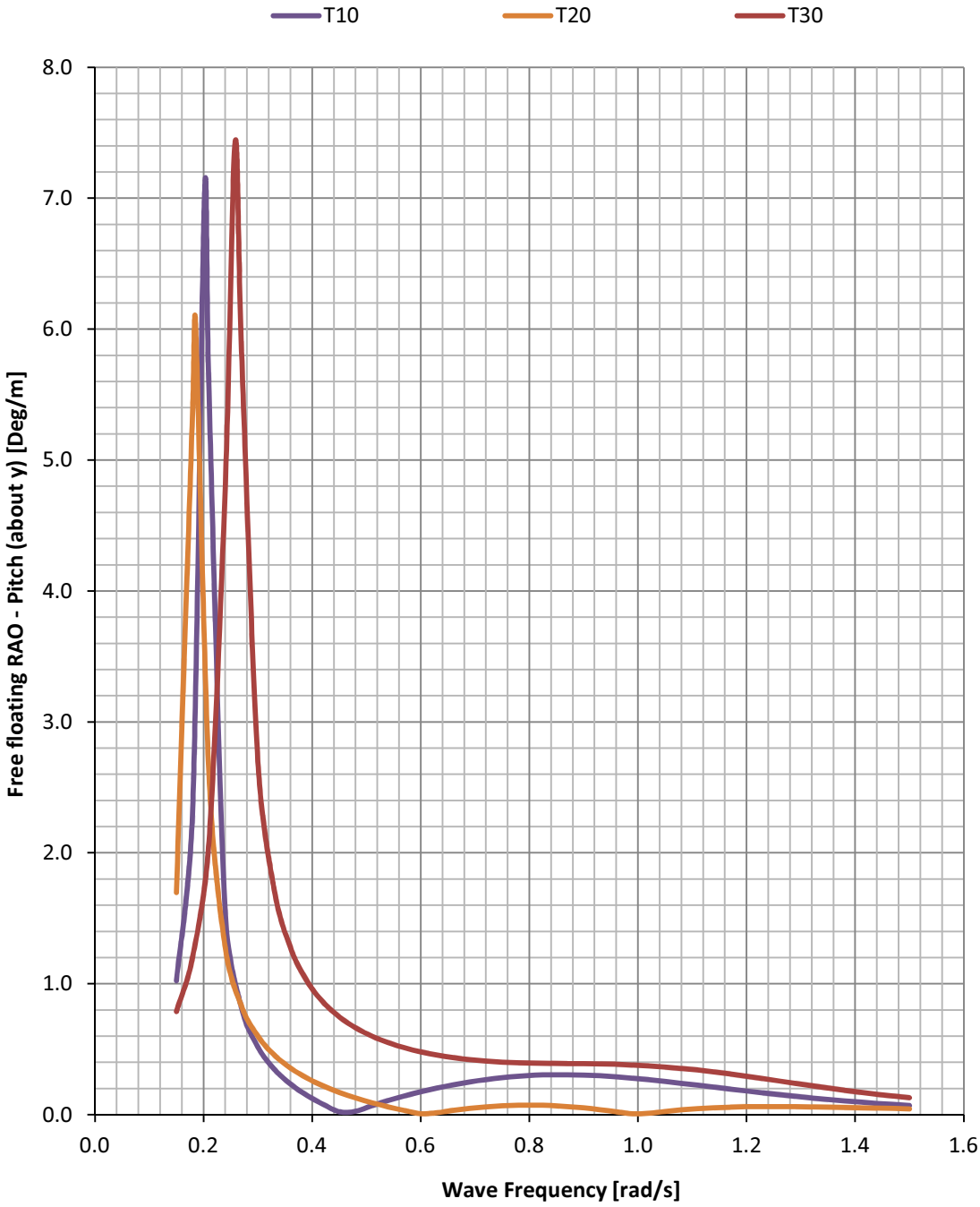

Figure 24: Free floating RAOs in pitch for T10, T20 and T30 (water depth d = 35 m)

3.3.4 Numerical Verification of the Natural Frequencies in Heave

The natural frequencies of the GBF in heave, determined with AQWA LINE, are validated in this section. The natural frequency is expressed by (Newman J. N., 1977)

$$\omega_{033} = \sqrt{\frac{c_{33}^*}{m_{33} + m_{h33}}} \tag{3.3}$$

The restoring constant c_{33}^* in heave of a semi submerged structure is defined by

$$c_{33}^{*} = \rho \cdot g \cdot A_{WL} \tag{3.4}$$

The hydrodynamic mass in heave $\mathrm{m_{h33}}$ is estimated for the disk at the base of the GBF with the radius $R = 19\,m$ (Clauss & Lehmann, 1992, S. 281).

$$m_{33h} = \frac{4}{3} \cdot \rho \cdot R^3 \tag{3.5}$$

The natural frequency in heave (3.3) is determined by the values in the table below:

Draft	Waterplane Area A_{WL} [m²]	Restoring Constant c_{33} [kN/m]	Structural Mass m_{s33} [t]	Hydrodynamic Mass m_{h33} [t]
T00	779.311	7836.17	6961.6	9374.0
T10	779.311	7836.17	7909.1	9374.0
T15	522.920	5258.09	11285.4	9374.0
T20	299.962	3016.20	13367.8	9374.0
T25	138.566	1393.31	14465.2	9374.0
T30	49.655	499.29	14900.9	9374.0
T33	31.557	317.31	15024.9	9374.0

Table 16: Determined input values for resonance frequency

The natural frequencies by hand and AQWA calculation are listed in the following table. Hand calculations of the natural frequency in heave show good conformity with results from AQWA calculations. Results from the model tests of the natural frequency also comply with the AQWA calculations.

Draft	Natural Frequencies ω_{033} [rad/s]	
	Hand Calculation	AQWA
T00	0.693	0.665
T10	0.673	0.646
T15	0.504	0.464
T20	0.364	0.322
T25	0.242	0.205
T30	0.143	0.113
T33	0.114	0.080

Table 17: Natural frequencies by hand and AQWA calculation

3.3.5 Maximum Motion

The amplitudes of maximum heave and pitch motion of the free floating GBF are determined by AQWA FER. This is done for all considered drafts and a range of wave spectra. Wave spectra are defined by their peak period T_P. Results are shown in Table 18 and Table 19 for peak frequency ω_P. The calculations are based on the previously determined ROAs

Draft / ω_P [rad/s]	T00	T10	T15	T20	T25	T30	T33
1.26	0.02	0.01	0.04	0.04	0.03	0.02	0.01
1.14	0.05	0.04	0.05	0.06	0.05	0.03	0.02
1.05	0.13	0.10	0.07	0.08	0.07	0.05	0.03
0.97	0.25	0.21	0.08	0.10	0.09	0.06	0.04
0.90	0.41	0.36	0.09	0.12	0.11	0.08	0.05
0.84	0.60	0.54	0.09	0.14	0.13	0.10	0.06
0.79	0.81	0.74	0.11	0.15	0.15	0.11	0.07
0.74	1.08	0.99	0.15	0.16	0.17	0.12	0.07
0.70	1.37	1.28	0.21	0.17	0.18	0.14	0.08
0.66	1.58	1.55	0.31	0.17	0.19	0.15	0.09
0.63	1.62	1.68	0.43	0.17	0.20	0.15	0.09
0.60	1.57	1.67	0.57	0.17	0.21	0.16	0.10
0.57	1.48	1.60	0.71	0.17	0.21	0.17	0.10
0.55	1.42	1.52	0.88	0.17	0.21	0.17	0.10
0.52	1.37	1.45	1.08	0.19	0.21	0.17	0.11
0.50	1.33	1.40	1.30	0.22	0.21	0.18	0.11
0.48	1.30	1.36	1.50	0.28	0.21	0.18	0.11
0.47	1.27	1.33	1.66	0.35	0.21	0.18	0.11
0.45	1.25	1.30	1.74	0.43	0.20	0.18	0.11
0.43	1.23	1.28	1.76	0.53	0.20	0.18	0.11
0.42	1.21	1.26	1.72	0.64	0.19	0.18	0.11

Table 18: Maximum heave amplitude $(s_{3.MAX})_a$ per significant wave amplitude ζ_{Sa} [m/m] over peak wave frequency ω_P

Draft / ω_P [rad/s]	T00	T10	T15	T20	T25	T30	T33
1.26	0.17	0.13	0.10	0.04	0.16	0.21	0.17
1.14	0.22	0.17	0.15	0.04	0.20	0.25	0.20
1.05	0.26	0.20	0.19	0.04	0.23	0.29	0.23
0.97	0.28	0.23	0.22	0.04	0.24	0.31	0.25
0.90	0.30	0.24	0.24	0.04	0.24	0.33	0.28
0.84	0.31	0.25	0.25	0.05	0.24	0.34	0.29
0.79	0.32	0.25	0.25	0.05	0.24	0.35	0.31
0.74	0.31	0.24	0.25	0.05	0.24	0.36	0.33
0.70	0.31	0.23	0.24	0.05	0.25	0.38	0.35
0.66	0.30	0.22	0.23	0.05	0.25	0.39	0.37
0.63	0.28	0.21	0.21	0.05	0.26	0.41	0.39
0.60	0.27	0.19	0.20	0.05	0.27	0.44	0.41
0.57	0.26	0.18	0.19	0.06	0.29	0.46	0.44
0.55	0.25	0.17	0.17	0.07	0.30	0.49	0.47
0.52	0.23	0.16	0.16	0.09	0.32	0.52	0.50
0.50	0.22	0.15	0.15	0.10	0.34	0.56	0.54
0.48	0.21	0.14	0.14	0.12	0.37	0.60	0.58
0.47	0.19	0.14	0.14	0.14	0.39	0.65	0.62
0.45	0.18	0.14	0.13	0.16	0.42	0.70	0.67
0.43	0.17	0.15	0.13	0.18	0.45	0.77	0.73
0.42	0.16	0.15	0.13	0.20	0.49	0.84	0.81

Table 19: Maximum pitch amplitude $(s_{5.MAX})_a$ per significant wave amplitude ζ_{Sa} [Deg/m] over peak wave frequency ω_P

3.3.6 Drift Forces

The mean wave drift forces as far field solution are determined by AQWA LINE (ANSYS, Inc., 2009e). The results of the free floating GBF in the considered drafts are depicted in Figure 25. It proves that drift forces show a distinct maximum at wave frequencies below 0.7 rad/s. With increasing draft the maxima decreases in magnitude and shifts towards the lower end of the considered frequency range. At wave frequencies above 0.7 rad/s a second increase of mean wave forces are seen. The magnitude of these maxima increases with draft until T15 is reached. Greater drafts lead to decreasing magnitude.

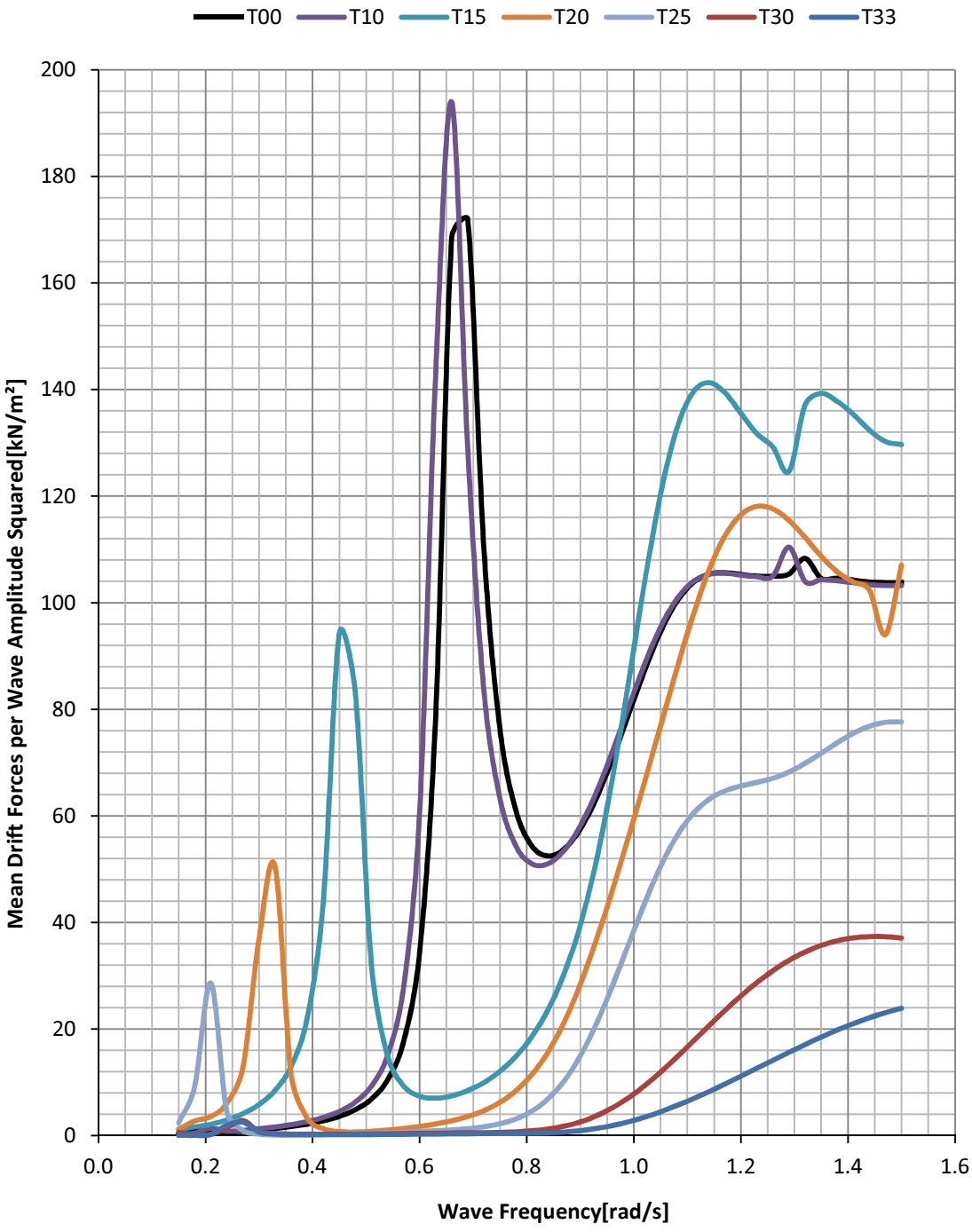

Figure 25: Mean drift forces per wave amplitude squared over wave frequency of all considered drafts (T00-T33) (water depth d = 35 m)

3.3.7 Tank Sloshing

A basic approach is made to determine the first order tank sloshing frequencies. Possible tank sloshing can be assumed when its frequency is in the range of high energy of the wave spectra. The resulting standing waves in the tanks could alter and possibly increase the foundations motion. In addition tank sloshing would promote tank overflow since tanks are open at the top.

The tank sloshing frequency is determined by the dispersion equation (2.12) and equation (2.13) on page 14. Here L is the wave length of a standing wave in the tank or twice the distance of adjacent tank walls and d the tank filling level (DNV, 2007). The maximal and minimal tank sloshing frequencies of the central tank and the outer tanks in relation to the tank filling level are shown in Figure 26.

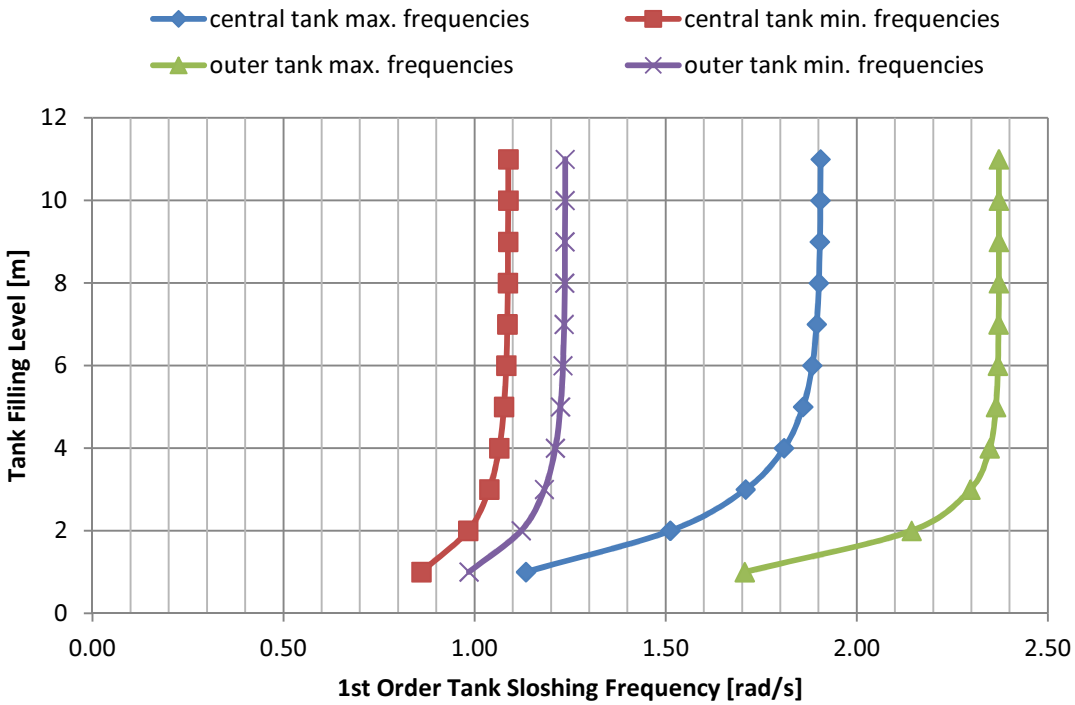

Figure 26: Approximated tank sloshing frequency in dependence of tank filling level

3.4 Motion Analysis in Time Domain

Analyses with AQWA NAUT are conducted in order to determine the impact of higher order effects of irregular sea states during the installation of the GBF. Model tests were conducted at DHI in Denmark.

3.4.1 Towing Tests

Results from model tests are taken to provide the required data to estimate the minimum required bollard pull BP. A calculation with AQWA LIBRIUM is taken for comparison. Note that AQWA LIBRIUM does not take into account the effect of forces of higher order such as drift forces.

The towing arrangement consists of the GBF in transit draft (T00) and two tug boats with a distance of 150 m from the mooring points. Tug boat 1 tows the structure with two mooring lines each with a linear stiffness of 88.29 kN/m. Tug boat 2 stabilises the towage by applying a constant force of 50 kN against the direction of towage.

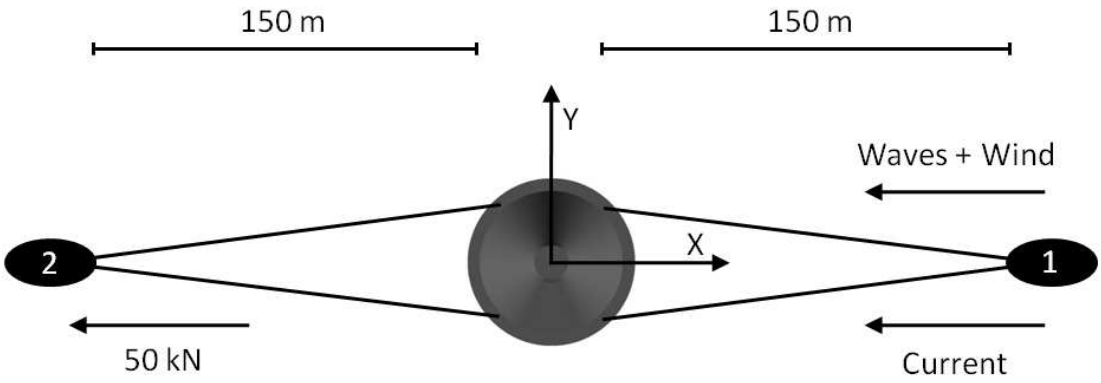

Figure 27: Towing arrangement

The holding conditions are applied with zero forward speed, 20 m/s wind, 0.5 m/s current and a water depth of 35 m. The simulated JONSWAP spectrum has significant wave height of 5 m and a peak frequency 0.79 rad/s. The results are shown in the following table.

		min	max	mean	std
Model Tests	Surge (x) [m]	-8.57	16.5	4.79	3.71
	Sway (y) [m]	-15.97	18.53	1.96	5.42
	Heave (z) [m]	-5.43	0.36	-2.29	0.83
	Roll (about x) [Deg]	-4.64	4.47	-0.17	1.14
	Pitch (about y) [Deg]	1.14	21.02	11.12	2.99
	Yaw (about z) [Deg]	-30.06	23.15	-4.87	14.12
	Mooring Force in X [kN]	0	2071	463	384
AQWA Librium	Pitch [Deg]	-	-	-0.83	-
	Mooring Force in X [kN]	-	-	492	-

Table 20: Towing test results for holding condition
($T00, H_S = 5\ m, \omega_P = 0.70\ rad/s, v_w = 20\ m/s, v_C = 0.5\ m/s$)

Additionally the equilibrium position during a towage at 1.5 m/s and 2.5 m/s in calm conditions is determined (Table 21) in order to estimate the associated inclination and mooring force. Calculations are made with AQWA LIBRIUM in the above towing arrangement.

Towing Speed [m/s]	**1.5**	**2.5**
Surge (x) [m]	-1.32	-2.86
Sway (y) [m]	0.10	0.03
Heave (z) [m]	1.51	1.29
Roll (about x) [Deg]	0.00	0.00
Pitch (about y) [Deg]	7.02	21.20
Yaw (about z) [Deg]	-0.03	-0.01
Mooring Force in X [kN]	227	631

Table 21: Equilibrium position at a towing speed of 1.5 m/s and 2.5 m/s and calm conditions

3.4.2 Installation Tests

In the installation tests set up the GBF model is moored between two tug boats holding it in place. The tug boats are implemented as fixed points at a distance of 150 m from the mooring points with a height of 1 m above still water level. Two mooring lines are used per tug boat with a linear stiffness of 88.29 kN/m each and a pretension of 50 kN in x-direction. Installation is simulated for a water depth of 35 m.

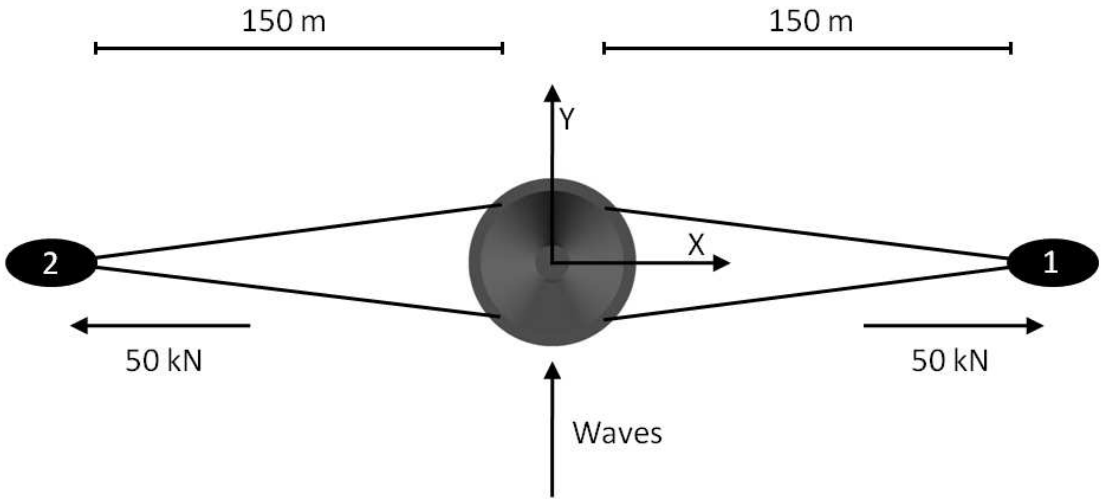

Figure 28: Installation set up

The applied seastate characteristics for the simulations are shown in Table 22. The simulation duration is set to 3 hours with a time step of 0.1 seconds. An additional prior 20 min build up phase of the motion is included in the simulation where no values are measured.

Installation Test No.	Draft	Significant Wave Height H_S [m]	Max. Heave (z) [m]	Max. Roll (about x) [Deg]
IT-1	T00	2	2.09	1.03
IT-2	T00	3	0.97	4.59
IT-3	T15	2	0.22	0.75
IT-4	T15	3	0.37	1.29
IT-5	T25	2	0.24	0.80
IT-6	T25	3	0.39	1.41
IT-7	T33	2	0.27	0.72
IT-8	T33	3	0.46	1.14

Table 22: Simulation set up and resulting maximum motions of installation tests ($\omega_P = 0.90\ rad/s$)

Maximum motions in heave and roll (about x) are also seen in Table 22. Complete results of each analysis are found in Table 28 to Table 35 (See Appendices).

3.5 Operation Limits

The gravity based foundation has to meet the following criteria for transit and installation (GL Nobel Denton, 2010).

3.5.1 Underkeel Clearance and Minimum Allowable Charted Water Depth

To prevent the GBF from colliding with the seabed during towage the following guidelines have to be fulfilled. The assumed minimum water depth of the port of construction is 10 m. At this water depth the transit water depth (T00) of the GBF is 8.82 m providing a 1.18 m underkeel clearance and exceeding the required 0.5 m.

The minimum allowable charted water depth during tow is the sum of the values in Table 23 below. This guideline accounts for the increase of draft through motions in waves. The minimum allowable charted water depth is 14.13 m in 2 m significant wave height and 14.94 m in 3 m significant wave height. Increase of draft through pitch motions is determined at an allowable maximum of 5°. For the increase of draft through heave motions the largest value in Table 18 is taken.

Significant Wave height H_S		**2**	**3**
Maximum static draft T [m]		8.82	8.82
Maximum increase of draft ΔT due to	Pitch and Roll (at 5°) [m]	1.69	1.69
	Heave [m]	1.62	2.43[17]
Underkeel clearance (UKC) [m]		2.00	2.00
Minimum allowable charted water depth [m]		14.13	14.94

Table 23: Minimum allowable charted water depth

3.5.2 Stability Requirements

The requirements, $\overline{GM_0} > 1\ m$ during transport (DNV, 1996/2000) and $\overline{GM_0} > 0\ m$ during installation (GL Nobel Denton, 2010), are met as seen in Table 5 on page 35.

Maximum inclinations are determined for pitch motion. Both in numerical simulation and in model tests the inclination limit of 5° is exceeded as seen in Table 24.

Test	**Model Test**
Maximum [Deg]	21.02
Minimum [Deg]	1.14
Mean [Deg]	11.12

Table 24: Pitch motions in holding condition

[17] Determined with the value for $H_S = 2\ m$ as followed: $s_{3max} = 1.62 \cdot H_S/2$

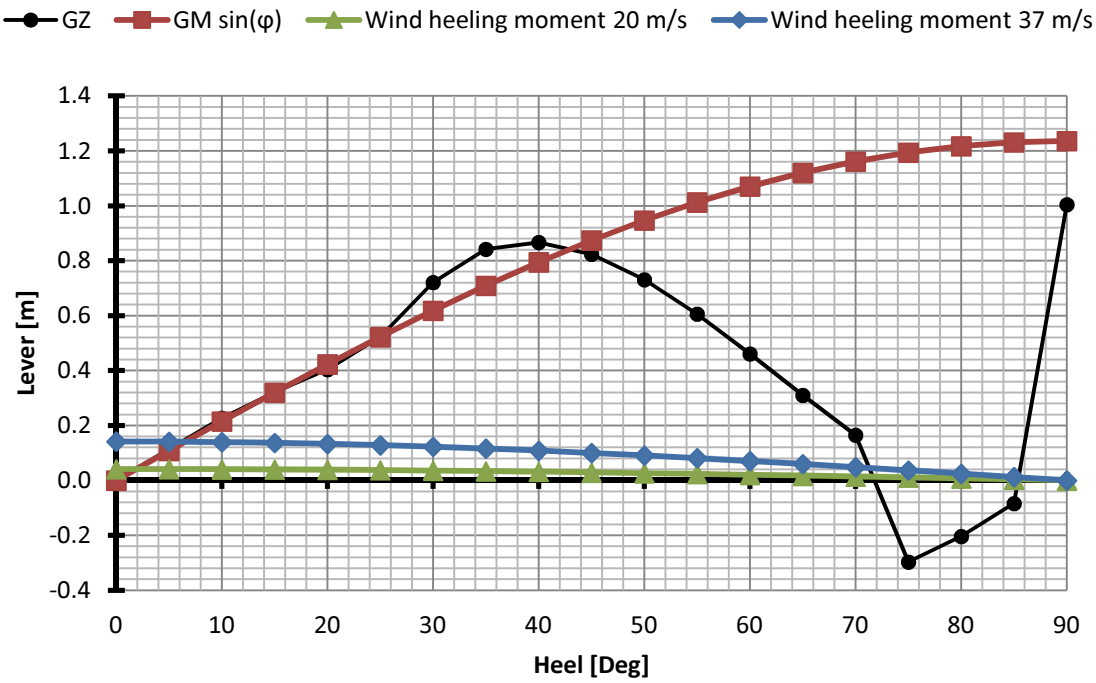

Figure 29: Righting arm curve of large angle and initial stability at transit draft T00 with wind heeling moments in holding condition (20 m/s) and in 1-year-return storm conditions (37 m/s) ($c_w = 1$)

The static range of stability during the towage is above 70° (see Figure 29) exceeding the required maximum[18] of 24° when the maximum allowable inclination θ_{max} is 5°.

When the GBF is subjected to 50% of TPR (equivalent to 272 kN, see Table 27) the static inclination must be smaller than 2°. The determined inclination is more than 7°, as shown in Table 21, and exceeds this limit.

The requirements for stability energy measured by the area ratio of righting and heeling curve are met. Results are shown in Table 25 for 37 m/s wind speed and a drag coefficient c_W of 1.

Area under righting moment curve A_{GZ} [mDeg]	35.16
Area under overturning moment curve A_{OM} [mDeg]	4.99
Relation A_{GZ}/A_{OM} [%]	705
Required Minimum Relation A_{GZ}/A_{OM} [%]	140

Table 25: Stability energy criteria

3.5.3 Tug Bollard Pull Requirement

The minimum towing pull requirement TPR of tug boat 1 in the holding condition[19] is 55.5 t. This includes a stabilising force of 50 kN of tug boat 2 against the direc-

[18] Required maximum static range of stability during the towage is determined by $20° + 0.8 \cdot \theta_{max}$

tion of towage. The tug boat efficiency T_e is 68.4%[20] determined by the guidelines in Table 26 (GL Nobel Denton, 2010).

Condition	Calm	$H_S = 2.0\ m$	$H_S = 5.0\ m$
BP < 30	80	50 + BP	BP
30 < BP < 90	80	80	7.5 + 0.75·BP
90 < BP	80	80	75

Table 26: Tug Efficiency T_e [%] in dependence of the bollard pull (BP) of the tug boat and the significant wave height H_S of the seastate (GL Nobel Denton, 2010)

The minimum required static bollard pull BP is determined by (3.6) is 81.2 t. This result complies with calculations made in other research work within the GBF project (Stempinski, 2011).

$$\mathrm{BP} = \frac{\mathrm{TPR}}{\mathrm{T_e}} \tag{3.6}$$

The determined towing characteristics are summarised in Table 27.

Static Towline Force [kN]	544
Min. Static Towline Pull TPR [t]	55.5
Tug Boat Efficiency T_e [%]	68.4
Min. Required Bollard Pull BP [t]	81.2

Table 27: Mooring forces at holding condition

4 Discussion

The discussion is divided into the following three sections: hydrostatic analysis, motion in frequency domain free floating GBF and installation limits.

4.1 Hydrostatic Analysis

The developed gravity based foundation shows adequate hydrostatic characteristics in regard to rules and regulations. At transport draft T00 the GBF is definite in shape due to the relatively large water plane area A_{WL} of the socket. With increasing draft the water plane area decreases and free surface effects of the tanks reduce stability (Figure 12). At drafts larger than 15 m, the GBF becomes definite in weight due to relatively low COG. Since an increasing amount of weight then originates from the ballast water in the tanks its even distribution in the tanks is crucial. Overflowing of the tank walls or linking of the tanks must be prevented in order to maintain a sufficient righting moment.

[19] towage at zero forward speed against 20 m/s wind, 5.0 m significant seastate and 0.5 m/s current simultaneously

[20] T_e depends on the size and configuration of the tug, the seastate considered and the towing speed achieved

The impact of the free surface effects on $\overline{GM_0}$ is considerable at the beginning of the lowering process where the central tank is flooded. At 10 m draft a second reduction $\overline{GM_0}$ occurs due to the flooding of the outer tanks. The significantly lower initial stability at T35 results from the overflowing of all tank walls and the subsequent increase of free surface moments. At that stage the foundation is close to the sea bed therefore possible inclination is limited due to touch down.

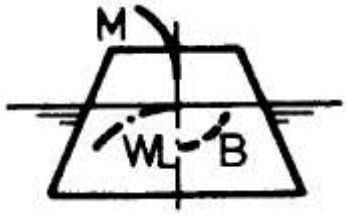

Figure 30: Stability characteristics of cone shaped structures (Schneekluth, 1988)

Overflow of the tanks and the immersion of the lower and upper cone of the GBF lead to a reduction of the $\overline{GZ}$-curve (Figure 29). The assumption that tanks are linked when the tank overflowing angle is reached, leads to greater reductions of the $\overline{GZ}$-curve. This is the case especially at a draft of 10 m (Figure 13). Here ballast water in the central tank shifts to the lowest point in the outer tanks. As a matter of fact, only the excessive water in the central tank flows into the outer tank thus causing a significantly smaller heeling moment. This effect becomes less critical with larger inclination and increasing ballast water. At drafts greater than 10 m the outer tanks are increasingly filled. The shift of ballast water is more limited thus causing smaller heeling moments.

4.2 Motion Analysis

The determined ROAs of pitch and heave motion in Figure 22 and Figure 23 show the three anticipated key characteristics: The approximation to 1 for declining wave frequencies, a peak at natural frequency and the approximation to 0 for growing frequencies. At small wave frequencies the encountered waves are long and the velocities and accelerations are small. The restoring forces prevail, causing the structure to follow the elevation of the wave in phase. At natural frequency, inertia forces and restoring forces are equal and cancel each other out. At this point damping forces determine the response which is 90° phase shifted to the oscillation of the wave forces. In short waves with high frequency, inertia properties prevent the structure from following the rapid changes of the excitation forces. Resulting oscillations are small and 180° phase shifted.

In transit draft T00 the natural frequency in heave is close to the considered peak frequencies of the wave spectrum and relatively high motions are seen Table 18. With increasing draft natural frequencies shift to lower frequencies, due to the dependence on decreasing water plane area and increasing total mass. Subsequently significant heave motions also decrease. A cancellation frequency can be recognised as minimum in the heave RAOs, next to the natural frequencies. At his point the up- and downward directed wave forces are equal and cancel each other out. This effect improves the hydrodynamic behaviour by reducing of maximum motion.

In the RAOs of pitch motion the dependence of the natural pitch frequency on $\overline{GM_0}$ can be seen. Since the peaks of natural pitch frequency are found at relatively low frequencies their impact on significant motion in the considered seastates is negligible. In the pitch RAOs cancellation frequencies can also be found. Analogous to the cancellation frequencies in heave, the effect originates from the cancellation of all pressure moments on the hull.

The effect of added viscous damping is limited to the maximum of the natural frequency and the minimum at cancelation frequency. An impact on significant motions in relevant sea states is therefore only seen in heave. The influence of additional viscous damping will decrease with increasing draft due to the shift in natural frequency. In cases where added viscous damping is without influence, the natural frequencies are located at low end of the wave spectrum.

The approximated frequencies of first order tanks sloshing are found in regions of high spectral energy. Model test however show no significant sloshing in the tanks. Thus the results of the numerical calculations, in which tank sloshing is disregarded, can be considered accurate.

The determined mean drift forces of the transit draft show a minimum at a wave frequency of 0.85 rad/s. If the peak frequency of the encountered wave spectrum is close to this point the resulting drift forces will be relatively small. This applies to the towing condition in $H_S = 2\ m$ with $\omega_p = 90\ rad/s$. Towing speed against the direction of wave propagation however will result in a increase of encountered ω_p. The peak of mean drift forces at higher end in this frequency range is then decisive. In regard to the lowering process decreasing mean drift forces are seen.

4.3 Towing and Installation Limits

During towage, the GBF conducts significant pitch motions, exceeding the limit of 5°. From equilibrium calculations it can be derived that current or towing speed in combination with the mooring forces on the base slab cause the structure to trim forward. This phenomenon is also seen in model tests. Since the centre of towing resistance is assumed to be located above the mooring points the resulting inclination is was expected in the opposite direction. In order to minimise pitch motion during towage the following structural solutions may be considered[21]:

- addition of counter weights,
- alteration of outer geometry to suppress the pitch effect,
- increase of $\overline{GM_0}$ or
- optimisation of the towing arrangement.

From the solutions offered above, addition of counter weights or the changes of outer geometry to suppress the pitch effect are the most promising alterations to the existing design of the GBF. By regulations the usage of counter weight is limited to static inclination 1° when the structure is free floating. This is equivalent to a moment of 1379 kNm or a total of 13.5 t of solid ballast homogeneously distributed in both aft tanks. Since the static angle is larger than 7° this measure is not

[21] Instrumental solutions are not considered due to design objectives of the GBF

sufficient. The pitch effect is assumed to be connected to the flow around the base slab. Alterations of the hull geometry in this region may be pursued in order to change the flow pattern.

During installation significantly smaller pitch and roll motions are identified. Since the angle of encounter is perpendicular to the direction of towing forces, roll motion dominates. In model test significantly larger motions are determined. An explanation may be found in the motion of the ballast water. This effect cannot be considered in AQWA. In regard to the determined heave motions, the bottleneck of the installation procedure is seen at the beginning of the lowering process.

Concluding from the gathered data an installation in 2 m significant wave height is assumed to be feasible. Suggestions concerning operation limits during towage are not made at this stage since deviations from the imposed limits are too significant. It is strongly believed that with overcoming pitching problems wave heights of 2 m will also be manageable during towing.

5 Appendices

5.1 Results of Installation Test with AQWA NAUT

IT-1	Motions Amplitudes						Mooring Forces		
	Surge [m]	Sway [m]	Heave [m]	Roll [Deg]	Pitch [Deg]	Yaw [Deg]	X [kN]	Y [kN]	Z [kN]
MAX	0.08	17.77	2.09	1.03	0.10	0.31	239	48	14
MIN	-0.08	-8.32	0.91	-1.63	-0.11	-0.30	46	0	2
Mean	0.00	5.54	0.00	-0.01	0.00	0.00	88	11	5
Standard Deviation	0.02	4.47	0.22	0.30	0.02	0.07	36	8	2

Table 28: Results of installation test no. IT-1 ($\boldsymbol{T00, H_S = 2\ m, \omega_P = 7\ rad/s}$)

IT-2	Motions Amplitudes						Mooring Forces		
	Surge [m]	Sway [m]	Heave [m]	Roll [Deg]	Pitch [Deg]	Yaw [Deg]	X [kN]	Y [kN]	Z [kN]
MAX	0.11	28.58	0.87	3.73	0.19	0.48	239	48	14
MIN	-0.09	-16.41	-0.97	-4.59	-0.19	-0.44	46	0	2
Mean	0.00	9.58	-0.01	-0.07	0.00	0.00	88	11	5
Standard Deviation	0.02	7.07	0.33	0.92	0.03	0.08	36	8	2

Table 29: Results of installation test no. IT-2 ($\boldsymbol{T00, H_S = 3\ m, \omega_P = 7\ rad/s}$)

IT-3	Motions Amplitudes						Mooring Forces		
	Surge [m]	Sway [m]	Heave [m]	Roll [Deg]	Pitch [Deg]	Yaw [Deg]	X [kN]	Y [kN]	Z [kN]
MAX	0.08	15.92	0.15	0.75	0.06	0.35	239	48	14
MIN	-0.09	-7.05	-0.22	-0.44	-0.08	-0.33	46	0	2
Mean	0.00	6.41	0.00	0.05	0.00	0.00	88	11	5
Standard Deviation	0.03	4.55	0.05	0.14	0.01	0.10	36	8	2

Table 30: Results of installation test no. IT-3 ($\boldsymbol{T15, H_S = 2\ m, \omega_P = 7\ rad/s}$)

IT-4	Motions Amplitudes						Mooring Forces		
	Surge [m]	Sway [m]	Heave [m]	Roll [Deg]	Pitch [Deg]	Yaw [Deg]	X [kN]	Y [kN]	Z [kN]
MAX	0.15	29.84	0.24	1.29	0.14	0.51	239	48	14
MIN	-0.12	-12.55	-0.37	-0.67	-0.17	-0.53	46	0	2
Mean	0.00	10.46	-0.01	0.07	0.00	0.00	88	11	5
Standard Deviation	0.04	7.88	0.07	0.24	0.03	0.15	36	8	2

Table 31: Results of installation test no. IT-4 ($\boldsymbol{T15, H_S = 3\ m, \omega_P = 7\ rad/s}$)

IT-5	Motions Amplitudes						Mooring Forces		
	Surge [m]	Sway [m]	Heave [m]	Roll [Deg]	Pitch [Deg]	Yaw [Deg]	X [kN]	Y [kN]	Z [kN]
MAX	0.07	12.06	0.22	0.57	0.03	0.28	239	48	14
MIN	-0.07	-2.89	-0.24	-0.80	-0.04	-0.29	46	0	2
Mean	0.00	4.60	0.01	0.03	0.00	0.00	88	11	5
Standard Deviation	0.02	2.75	0.06	0.15	0.01	0.08	36	8	2

Table 32: Results of installation test no. IT-5 ($T25, H_S = 2\ m, \omega_P = 7\ rad/s$)

IT-6	Motions Amplitudes						Mooring Forces		
	Surge [m]	Sway [m]	Heave [m]	Roll [Deg]	Pitch [Deg]	Yaw [Deg]	X [kN]	Y [kN]	Z [kN]
MAX	0.11	20.21	0.33	1.02	0.06	0.46	239	48	14
MIN	-0.11	-8.32	-0.39	-1.41	-0.09	-0.46	46	0	2
Mean	0.00	8.25	0.02	0.04	0.00	0.00	88	11	5
Standard Deviation	0.05	5.24	0.09	0.26	0.01	0.17	36	8	2

Table 33: Results of installation test no. IT-6 ($T25, H_S = 3\ m, \omega_P = 7\ rad/s$)

IT-7	Motions Amplitudes						Mooring Forces		
	Surge [m]	Sway [m]	Heave [m]	Roll [Deg]	Pitch [Deg]	Yaw [Deg]	X [kN]	Y [kN]	Z [kN]
MAX	0.02	2.15	0.27	0.57	0.02	0.01	246	45	15
MIN	-0.02	-1.14	-0.04	-0.72	-0.02	-0.01	95	0	5
Mean	0.00	0.59	0.09	0.01	0.00	0.00	151	45	9
Standard Deviation	0.00	0.59	0.09	0.01	0.00	0.00	123	11	7

Table 34: Results of installation test no. IT-7 ($T33, H_S = 2\ m, \omega_P = 7\ rad/s$)

IT-8	Motions Amplitudes						Mooring Forces		
	Surge [m]	Sway [m]	Heave [m]	Roll [Deg]	Pitch [Deg]	Yaw [Deg]	X [kN]	Y [kN]	Z [kN]
MAX	0.03	3.85	0.46	0.82	0.02	0.04	246	45	15
MIN	-0.03	-0.88	-0.13	-1.14	-0.02	-0.04	95	0	5
Mean	0.00	1.36	0.12	0.01	0.00	0.00	123	11	7
Standard Deviation	0.01	0.80	0.07	0.23	0.01	0.03	36	8	2

Table 35: Results of installation test no. IT-8 ($T33, H_S = 3\ m, \omega_P = 7\ rad/s$)

5.2 Wave Patterns

In the following figures the wave pattern of the diffracted and radiated wave are seen:

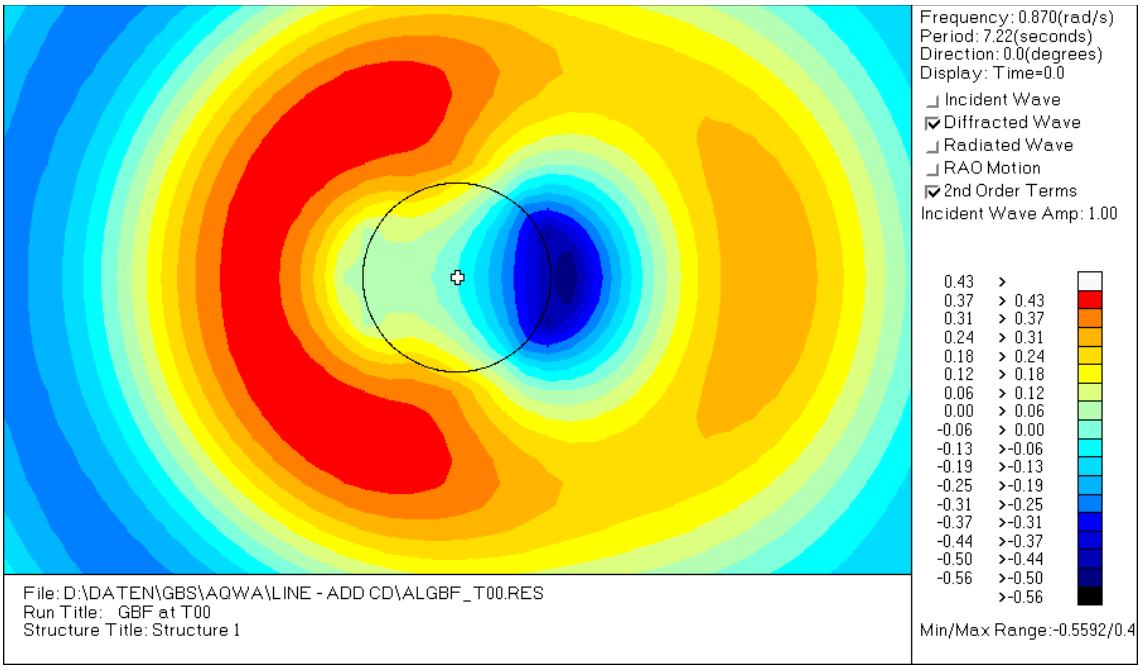

Figure 31: Diffraction wave field in regular waves ($t = 0\ s, \omega = 0.870\ rad/s$)

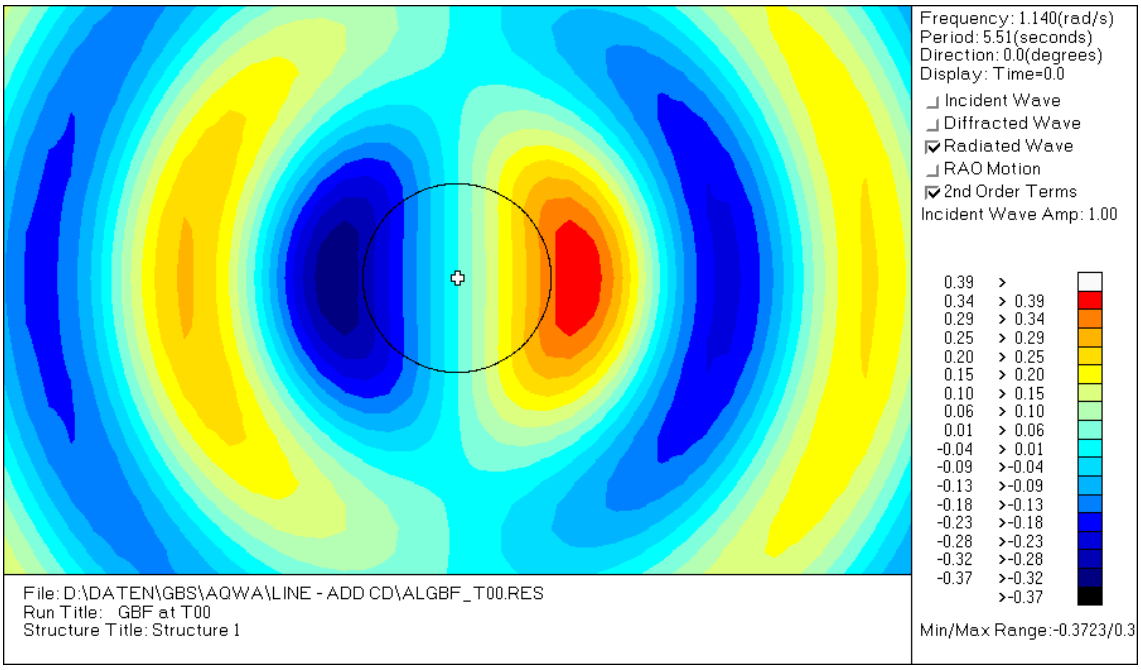

Figure 32: Radiation wave field in regular waves ($t = 0\ s, \omega = 1.140\ rad/s$)

List of Figures

List of Tables

References

ANSYS, Inc. (2009a). AQWA Reference Manual - Version 12.1. *Manual* , Manual.

ANSYS, Inc. (2009b). *AQWA Trainings Course.*

ANSYS, Inc. (2009c). *AQWA ™-FER MANUAL Release 12.0.*

ANSYS, Inc. (2009d). *AQWA ™-LIBRIUM MANUAL Release 12.0.*

ANSYS, Inc. (2009e). *AQWA ™-LINE MANUAL Release.*

ANSYS, Inc. (2009f). *AQWA ™-NAUT MANUAL Release 12.0.*

Arup, Constain, HOCHTIEF. (2011). *Concrete Gravity Bases Database.* Hamburg.

Birk, L. (2001). *Diffraktionstheory.* Berlin: FG Meerestechnik TU Berlin.

Bronstein, I. N., & Semendjajew, K. A. (1993). *Taschenbuch der Mathematik 1. Auflage.* G. Grosche & V. Ziegler.

Chen, X.-B. (2006). *The set-down in the second-order Stokes' waves.* France: Bureau Veritas - Research Department.

Clauss, G. F., & Lehmann, E. Ö. (1992). *Offshore Structures Vol. 1.* Berlin, Heidelberg, New York, Paris, Tokyo: Springer-Verlag.

Clauss, G. (1995). *Lecture Notes to Stochastische Analyse meerestechnischer Systeme.* Berlin: Technical University of Berlin.

Dasdeler, M. (2011, Oktober 17). Foundation Installation Duration. HOCHTIEF Solutions AG. Hamburg.

Deutsche Energie-Agentur GmbH (dena). (2009). *Fundamente für Offshore-Windenergieanlagen.* Berlin.

DHI. (2011). *Concrete Gravity Base Foundations for Offshore Wind Frams - Tank testing of Tow and Installation - Draft.*

DNV. (2007). *Environmental Conditions and Environmental Loads DNV-RP-C205.*

DNV. (1996/2000). *Rules for Planning and Execution of Marine Operations (Part 1, Chapter 2, Clause 4.3.2.1).*

European Wind Energy Association (EWEA). (2009). *www.ewea.org*. Retrieved Oktober 27, 2011, from www.ewea.org/fileadmin/ewea_documents/documents/publications/reports/European_Offshore_Wind_Map_2009.pdf

GL Nobel Denton. (2010). *Concrete Offshore Gravity Structures 0015/ND Rev 2.*

GL Nobel Denton. (2010). *Guidelines for Marine Transportation 0030/ND Rev 4.*

Goda, Y. (2000). *Random Seas and Design of Maritime Structures (2nd Edition).* World Sientific Publishing Co. Pte. Ltd.

HOCHTIEF Solutions AG. (2011). *Database of the Offshore Division.* Hamburg.

Houmb, O., & Overvik, T. (1976). Parametrization of Wave Spectra and Long Term Joint Distribution of Wave Height and Period. *First International Conference on Behaviour of Offshore Structures (BOSS).* Trondheim.

IMO. (2009). *Maritime Safety Committee - 85th session - Agenda item 26.*

Journée, J., & Massie, W. (2001). *Offshore Hydromechanics - First Edition.* Delft University of Technology.

Lee, C. (1995). *Wamit theory manual. Technical report, Massechusetss Institue of Technology. Preliminary Copy.*

Lewis, E. (1989). *Principles of Naval Architecture (Second Revision), Volume III - Motions in Waves and Controllability.* Jersey City: Society of Naval Architects and Marine Engineers (SNAME).

Mei, C. C. (1989). *The Applied Dynamics of Ocean Surface Waves.* Singapore: World Scientific.

MetOcean. *MetOcean Report.*

Newman, J. N. (1977). *Marine Hydrodynamics.* N/A: MIT Press.

Newman, J. (1967). The Drift Force and Moment on Ships in Waves. *Journal of Ship Research, Vol. 11* , 51-60.

Newmann. (1977). *Marine Hydrodynamics.* Cambridge, Massachusetts: M.I.T. Press.

Schneekluth, H. (1988). *Hydrodynamic zu Schiffsentwurf - 3. Auflage.* Hamburg: Koehler Verlag.

SMart Wind. (2011). *www.smartwind.co.uk*. Retrieved November 25, 2011, from http://www.smartwind.co.uk/the-zone.aspx

Stempinski, D.-I. F. (2011). GBF Project. (M. P. Bense, Interviewer)

Wehausen, & Laitone. (1960). *Surface Waves, In Encyclopaedia of Physics, Vol. IX, pp. 446-778 of Fluid Dynamics III.* Berlin: Springer Verlag.

Table of Acronyms

BP	Bollard Pull
COB	Centre of Buoyancy
COG	Centre of Gravity
DNV	Det Norske Veritas
FRA	Fixed References Axis
GBF	Gravity Based Foundation
LAT	Lowest Astronomical Tide
QPPL	Quadrilateral Pressure Plate Element
TPPL	Triangular Pressure Plate Element
TPR	Towing Pull Requirement

Table of Abbreviations

Symbol	Name	SI-Unit
Γ	Euler integral	-
ΔL	Extension oft the mooring line	m
Φ	Total potential of the wave field	m²/s
Φ_0	Velocity potential of singular initial harmonic wave	m²/s
Φ_7	Diffraction potential	m²/s
Φ_D	Total diffraction potential	m²/s
Φ_l	Radiation potential of the 6 degrees of freedom	m²/s
γ	Peak enhancement factor	-
γ_j	Phase shift of excitation force F_{ej} in the degree of freedom j	rad/s
ε	Radius of the (hemi-)sphere surrounding $\underline{x}$	m
ϵ_j	Phase shift of motion s_{ja} in the degree of freedom j	rad/s
ζ_a	Wave amplitude	m
θ	Angle of trim	Deg
$\underline{\xi}$	Vector of source point located on the body surface	m

Symbol	Name	SI-Unit
ρ	Mass density of salt water	kg/m³
ν	Kinematic viscosity	m/s²
φ	Angle of heel	Deg
φ_l	Radiation velocity potentials	-
χ	Funktion of wave encounter	m
ψ	Angle of encounter	Deg
ω	Wave frequency	Deg
ω_m	Centre of area of the spektral packet	rad/s
ω_P	Peak frequency of the wave spectra	rad/s
ω_{Rj}	Natural frequency in the degree of freedom j	rad/s
A_S	Projected area below water level	m²
A_W	Projected area exposed to wind	m²
A_{WL}	Water plane area	m²
AR	Aspect ratio	-
B	Damping matrix	-
B_0	Initial centre of buoyancy	-
B_j	Damping in the degree of freedom j	-
B_φ	COB of the inclined structure	-
$\overline{BM}_0$	Initial metacentre above centre of buoyancy	m
C	Stiffness matrix	-
C_{ML}	Stiffness matrix of mooring line at attachment point on the structure	-
D	Mean drift coefficient	-
E	Space inside considered Space V_C and S	m⁴
F	Total forces	N
F_B	Buoyancy force	N

Symbol	Name	SI-Unit
F_D	Mean drift force	N
F_{Drag}	Drag force	N
F_G	Weight force	N
$\underline{F_e}$	Excitation force on the structure	N
F^*_{eja}	Force amplitude in the degree of freedom j	N/m
$F_{ej}{}^*$	complex response amplification function of the excitation forces in the degree of freedom j	N/m
F_H	Hydrostatic force	N
F_{ml}	Mooring forces at the attachment points	N
F_{ML}	Mooring forces at COG	N
F_W	Wind drag force	N
F_{wf}	Total wave frequency force	N
G	Centre of gravity	-
$\mathfrak{G}$	Second Green Function	-
$\overline{GB}_0$	COG above initial COB	m
$\overline{GM}_0$	Centre of metacentric height	m
$\overline{GZ}_\varphi$	Righting lever	m
H	Wave height	m
H_{max}	Maximal wave height	m
H_s	Sginifcant Wave Heitght	m
H_j	Response amplification factor in the degree of freedom j	-
I	Unit matrix	-
I_T, I_L	Transvers and longitudinal second moment of water-plane area	m^4
I_{Ti}, I_{Li}	Transvers and longitudinal second moment of free surface area of tank i	m^4
I_{xx}, I_{yy}, I_{zz}	Second moment of inertia about x-, y- and z-axis	m^4

Symbol	Name	SI-Unit
I_ε	Integral over the (hemi-)sphere surrounding $\underline{x}$	-
J_0	Bessel function	-
$\overline{KB}$	COB above moulded base or keel	m
$\overline{KG}$	COG above moulded base or keel	m
$\overline{KM_0}$	Metacentre above base or keel	m
L	Wave length	m
L	Unstretched length of the mooring line	m
$\overline{M_0N_\varphi}$	Prometacentre N_φ above metacentre M_0	m
M_0	Initial metacentre	-
M_φ	Metacentre	-
M_{Drag}	Drag moment	*Nm*
M_h	Hydrodynamic mass matrix	-
M_{hj}	Added mass matrix at ω_j	-
M_R	Rigthing moment	*Nm*
M_W	Wind overturning moment	*Deg*
M_s	Structural mass matrix	-
N	Number of panels	-
N_φ	Prometacentre	-
N_S	Number of samples in a cycle	-
N_{SPL}	Number of regular wave components in the wave spectrum	-
N_W	Number of waves in a wave train or wave record	-
P_0	Pretention oft the mooring line	*N/m*
P_{ML}	Force of the mooring line	*N/m*
$\underline{P}$	Linear momentum	
Rn	Reynolds-number	-

Symbol	Name	SI-Unit
S	Spectral ordinate	-
S_∞	Control surface V_C in the xz- and xy-plane	m^2
S_B	Sea bed	m^2
S_F	Water surface	m^2
S_b	Body surface	m^2
S_k	Panel surfaces	m^2
T_p	Peak period	s
V	Displacement	m^3
V_C	Control volume	m^3
b_{cij}	Critical damping coefficient in degree of freedom i originating from motions j	-
b_{ij}	Total damping coefficient in degree of freedom i originating from motions j	-
b_{pij}	Potential damping coefficient in degree of freedom i originating from motions j	-
b_{vij}	Viscous damping coefficient in degree of freedom i originating from motions j	-
c_h	Height coefficient	-
c_D	Drag coefficient	-
c_{ij}	Stiffness coefficient in degree of freedom i originating from motions j	-
c_s	Shape coefficient	-
d	Water dephts	m
f_j	Complex total wave force at ω_j	-
g	Gravity	m/s^2
h_{WP}	Vertical lever of the wind overturning moment	m
h_w	Normalised wind overturning moment	m
k	Wave number	m^{-1}

Symbol	Name	SI-Unit
k_H	Harmonic component	-
k_{ML}	Linear stiffness of mooring line	*N/m*
k_{bij}	Damping Factor	-
$\underline{l}$	Vector joining the attachment points of the mooring line	-
m_{hij}	Structural mass in degree of freedom i originating from motions j	-
m	Spectral area	
m_1	First moment of area of the spectral energy	*rad/s*
m_{hij}	Hydrodynamic mass in degree of freedom i originating from motions j	-
$\underline{n}$	Normal vector on limiting surfaces S of control volume V_C	-
n_k	Normal vector of panels	
p	Dynamic pressure	*N/m²*
p_{stat}	Hydrostatic pressure	*N/m²*
r	$= \underline{x_i}$	*m*
r_f	Facet radius	*m*
$\underline{s}$	Position vector	*m*
$\underline{\dot{s}}$	Velocity vector	*m/s*
$\underline{\ddot{s}}$	Acceleration vector	*m/s²*
s^*	Complex motion response amplification function in the degree of freedom j	-
s_{MAXa}	Maximum motion amplitude	*m*
s_{ja}	Motion amplitude in the degree of freedom j	*m*
s_{Sa}	Significant motion amplitude	*m*
t	Time	*s*
u_n	Normal velocity of the surface	*m/s*
$\underline{v}$	Vector of fluid velocity of fluid on surfaces	*m/s*

Symbol	Name	SI-Unit
v_ψ	Angular fluid velocity of fluid on surfaces	*m/s*
v_c	Current velocity	*m/s*
v_l	Structure velocity in the degree of freedom l	*m/s*
v_n	Normal fluid velocity of fluid on surfaces	*m/s*
v_r	Radial fluid velocity of fluid on surfaces	*m/s*
v_W	Wind speed	*m/s*
$\underline{x}$	Vector point located in V_C	*m*
$\underline{x_B}$	Position vector of COB	*m*
$\underline{x_G}$	Position vector of COG	*m*
$\underline{x_i}$	Vector of control point	*m*
$\underline{x_k}$	Panel control point	*m*
$\underline{\mathrm{x_{ML}}}$	Vector of attachment point oft the mooring line on the structure	*m*
$\mathrm{x_p}$	distance from the origin of the wave system perpendicular to the wave direction	*m*
$\underline{\mathrm{x_{SWL}}}$	Vector of the centre of waterplane area A_{WL}	*m*
$\mathrm{z_{CUR}}$	Vertical lever of the drag force	*m*